Characterisation and Antibacterial properties of modified bentonites in animal litter application

Cumont Aude, M2 IMACS 2017
Supervisors: Dr G. Christidis and Dr. D. Venieri

Summary

Abstract

Two Bentonites from Milos Island, Greece, were characterised and modified in order to develop antibacterial animal litter. Rema Bentonite is a poor quality bentonite containing 29% montmorillonite of low layer charge. Its clay fraction is composed of montmorillonite, muscovite and clay size clinoptilolite, which confers great CEC (56.3 meq/100g) compared to the smectite content. FTIR and XRF analysis confirm the presence of montmorillonite with Mg and Fe substitutions, with K-rich interlayer, in accordance with its volcanic ash weathering origin. S2 bentonite is a good quality bentonite consisting of 70% low layer charge beidellite. FTIR and XRF confirm Mg and Fe substitutions in the lattice and Na-rich interlayers that is in accordance with its natural tendency to form stable suspension when added in water. Its measured CEC is 60.9 meq/100g.

Both Rema and S2 bentonites were modified with known antibacterial agents. Cu-modified bentonites and Ag-modified bentonites were prepared through cation exchange with a solution concentration of 1% of respective CEC. The presence of these cations in interlayer is verified with XRD bulk sample analysis. Al-modified and B-modified bentonites does not contain these cations in interlayer. They are in porous water after overnight contact time.

The antibacterial properties of natural and modified bentonites were assessed through MIC and MBC experiments on *S. aureus* (gram +)*, P. aeruginosa* (gram -)*, E. coli* (gram -) and *K. pneumoniae* (gram -). Natural Rema bentonite does not have strong antibacterial properties but modified Rema bentonites have strong. The best "dopant" is silver but because of its toxicity and light reduction in $Ag_{(s)}$ nanoparticles, it is not advised to use it as animal litter. Copper, Aluminium and Boron have great bacteriostatic and bactericidal effect that are dose and gram-type dependent. Natural S2 bentonite has strong bacteriostatic and bactericidal effect thanks to an unknown antibacterial component. Modification did not enhanced significantly its antibacterial action. Toxicity assessment on natural interlayer antibacterial compound is needed, but the results show that the material might be an animal litter great antibacterial properties. The development of animal litter based on this two bentonites is possible and modification depends on company wishes. In addition, it is probably possible to develop an antibacterial clumping litter based on the S2 bentonite and an antibacterial litter without clumping behaviour based on Rema bentonite

Introduction

Because of the intensive way of life in developed countries, meat and dairy products consumption is increasing and will continue to increase (Mathijs 2015, Sans et al. 2015). In this context, livestock farming is an expanding activity, more and more oriented to intensive and battery farming. Consequently, litter plays an increasing role into these activities, and even for extensive breeding during winters or nights. The major functions of litter are: absorption of urine and desiccation of defecation, control of dejection smells and vapours, and health control (by drying the environment, litters hinter the development of potential common pathogens and smells). Properties required include low toxicity and production of the minimum possible quantity of dust to avoid lung injuries (Zilaout et al. 2017). Keeping dry environments is also of great importance to avoid reproduction of common pathogens and high-scale contamination of livestock and thus reduce the need for antibiotics during breeding and consequently the appearance of antibiotic-resistant pathogens (Villa et al. 2016, Dodds, 2017) and finally the potential transmission of diseases to humankind (Trevisi et al 2014). In addition, decomposition of urea produces ammonia emanations that are very toxic for the lungs of cattle and humans (Canadian Centre of Work Hygiene and Security, classification SIMDUT 1988 of ammoniac: D1A: Very toxic material and E: Corrosive material). In this context, creation of high quality litters is of great importance. Furthermore, these problematics can also be applied to pet owners, and

especially of cat owners. In this specific case, an additional parameter has to be taken into account: the litter toxicity level has to be carefully controlled because of swallowing risks for young children and for cat during grooming routine, especially paws licking.

Different types of litter are now available on the market for pet owners and they are mainly based on plant- or mineral-pellets. Mineral litters are based on aluminosilicate minerals and two main types are available. The first one is composed of zeolite white crystals and the second one is based on clays, mainly bentonites.

Bentonites is an industrial clay of great importance and with numerous industrial applications including animal litters. The properties of bentonite are inherited from its major clay component, smectite. Smectite is a 2:1 layer phyllosilicate (Al-octahedral sheet sandwiched between two Si-tetrahedral sheets creating 2:1 units separated by an interlayer) with swelling properties (Barral et al. 2016, Cui 2017) and high specific surface area (Kaufhold et al. 2017). The swelling property allows bentonite to be hydrated and dehydrated and imparts liquid adsorption properties. In addition, cation exchange capacity of smectite (and hence of bentonite) is usually high (Shiffman et al. 1996), which allows bentonite to be doped with cations. Furthermore, the high specific area allows smectite interlayers to interact with organic compounds for example, which can be stored in smectite interlayers and then released when necessary. Smectites and, consequently bentonites, are very reactive minerals that can be easily chemically modified for special applications.

In this context, this study focuses on the antimicrobial properties of clay nanoparticles for cat-litter use. A cat litter can rest in cat litter box for more than one month depending on the quality of the litter and its clumping properties. Even if the owner removes every day excretions and clumps composed of urine and litter, dirty pellets which could remain in the litter box, might pose a potential risk for pet and human health. One of these potential risks is ammonia vapour emanation product of urea hydrolysis. The ammonia vapour, as previously said, might cause lungs injuries to young children or pets. Another potential risk is the development of pathogenic microorganisms, even if the litter ensures the better possible drying of the litter box. Microorganisms may also be responsible for the production of ammonia emanations because numerous microorganism species produce urease, which is an enzyme able to catalyse urea hydrolysis. Considering these parameters and knowing that cats, even if they wash themselves often, can be a vector of dispersion of microorganisms, give antibacterial properties to cat-litter is an interesting way to ensure a healthier environment. In a larger scale, extend these properties for livestock litters, could reduce antibiotic use and the appearance of antibiotic-resistant microorganisms.

In an economic and market point of view, "Akrolithos" company, which already produces cat-litter "Terracat" wishes to increase its market share with a new product: antimicrobial litter. In order to reach this goal, "Akrolithos" company supplied two Terracat mineral litter samples. In a multidisciplinary perspective, these samples will be carefully characterised, doped with antibacterial agents and finally tested on four bacteria species.

Material and Methods

1) Supplied samples and mineralogical characterisation
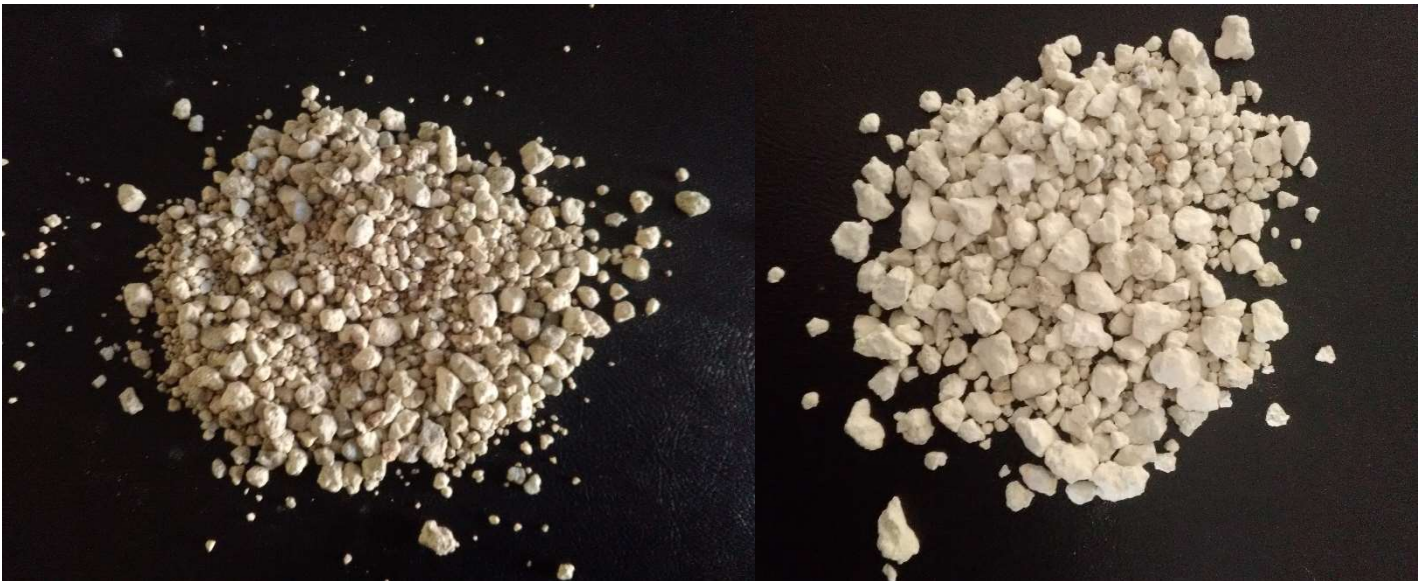
a) Macroscopic characteristics

Figure 1: S2 (left) and Rema (right) samples observed to the naked eyes

Two bentonite animal litter samples with 7.5mm grain size were supplied by Akrolithos Co. The bentonites are available in the market with the brand name Terracat. The first bentonite is from Rema deposit in Milos Island (hereby denoted as REMA), is nearly white, and shows a good dispersion behaviour when crushed and added into water. It is a soft material, producing dust when shacked and with clayey deposit on hands.

The second bentonite sample also from Milos Island comes from the area of Aspro Horio and was supplied by the Hellenic Mining Company (EME), (hereby denoted as S2). It is a sticky brownish material. It does not produce dust when shacked and agglomerates when added into water. It clearly needs sonication to disperse into water and forms immediately a stable suspension without flocculation.

b) X-ray diffraction procedure
The bulk samples was analysed in randomly oriented powder and the clay fraction in oriented slides.

- *Randomly oriented powder preparation*

The bulk fraction is ground as fine as possible in an agate mortar. The powder holder is covered with a glass slide, and the obtained powder can be added only by a littleslit in the side, avoiding orientation of particles. It is tapped regularly to obtain a compact powder. The glass slide ensure a smooth surface. When samples are prepared, they are protected from potential dust contamination. Peaks were identified with EVA software and quantification analysis was performed with AutoQuan software.

- *Extraction of the < 2 µm fraction*

10 g of sample is crushed and inserted into a 150 mL beaker. The suspension is dispersed with ultrasonication for 30 seconds and rests for 48 minutes for sedimentation of particles. This time was determined with the Stokes' law and allowed to extract the first centimetre which contains the < 2 µm fraction. Subsequently, distilled water was added again to the 150mL graduation, the suspension is sonicated again and allowed to rest for another 48 minutes.

This cycle was repeated until the first centimetre appears as limpid as clear water or until enough clay fraction was recovered for following analyses.

- *Clay saturation procedure*

Preparation of solutions used for the saturation

Three saturations are done: Li saturation, Cs saturation and K saturation.

In order to perform these saturations, 3 stock-solutions containing different cations with concentration of 1 mol.L^{-1} (1M) were prepared:

- Li solution: 21.20g of $LiCl_{(s)}$ were placed into a 500 mL flask. Then, about 100mL of distilled water were added. The solution was stirred and after dissolution of the salt, distilled water was added to the 500mL mark. The solution was stirred again to homogenise.
- K solution: 37.28g of $KCl_{(s)}$ salt were placed into a 500 mL flask. Then, about 100mL of distilled water were added. The solution was stirred and after dissolution of the salt, distilled water was added to the 500mL mark. The solution was stirred again to homogenise.

- Cs solution: 84.18g of $CsCl_{(s)}$ salt were placed into a 500 mL flask. Then, about 100mL of distilled water were added. The solution was stirred and after dissolution of the salt distilled water was added to the 500mL mark. The solution was stirred again to homogenise.

Saturation of the clay fraction

For each cation saturation: 2 mL of the clay fraction were put in centrifugation tubes and 10 mL of the cation solution were added. The obtained suspension was shaked and left for saturation overnight. Then, the suspension was centrifuged at 7000 rpm for 7 minutes. If clay remains in supernatant after centrifugation, rotation speed was increased to 9000 rpm. The supernatant was carefully removed and distilled water was added to wash the clay fraction. The suspension was sonicated to disperse the clay sediment into water and was centrifuged again at 7000 rpm (or 9000 rpm, depending of the presence of clays or not in the supernatant) for 7 minutes. Then, the supernatant was removed, distilled water was added and the suspension is sonicated again. This washing cycle was repeated 5 times to remove excess Cl^- anions and finally was tested with $AgNO_3$ reagent. If white precipitation appears, Cl^- ions are present in the supernatant and the washing procedure has to continue until the $AgNO_3$ test is negative.

- *Preparation of oriented slides for X-ray diffraction analysis*

Case of K-saturated clays, Cs-saturated clays and unsaturated clay fraction

1 mL of clay suspension was placed on a glass slide. The bentonite clay suspension had to be concentrated enough so that the sample code, below the slide is visible but not readable. If the bentonite suspension is more concentrated, clays might roll during drying. If it is not enough concentrated, X-ray diffraction traces will be noisy. The slide was then air dried. The clay coating of slides was verified after drying to avoid any rolling or holes.

Case of Li-saturated clays

The suspension of Li-saturated clays was dried at 60°C in an oven overnight. Then the collected powder was heated at 300°C for 12 hours. The dried homoionic clay was crushed, and dispersed in distilled water with ultrasonication. Then 1 mL of saturated clay suspension was put on a glass slide.

Natural clay and K-saturated clay oriented slides were saturated with ethylene glycol vapours. The oriented slides were placed in an evaporator containing liquid ethylene glycol. The device was heated at 60°C in an oven overnight (at least 16 hours) to saturate evaporator atmosphere and ensure ethylene glycol saturation of the samples. The Cs-saturated and Li-saturated oriented slides were placed in an evaporator containing liquid glycerol. The evaporator was heated at 100°C 20h to saturate evaporator atmosphere with glycerol and ensure glycerol saturation of the samples.

Aim of different saturations

K saturation allows estimating the smectite layer charge. Actually high charge smectites (like in case of illitisation weathering) will induce dehydration of K cation in their interlayer, causing partial collapsing even with ethylene glycol saturation. In contrast, low charge smectites (below -0.425 e/huc, Christidis & Eberl, 2003) smectites will not induce this dehydration and continue to swell with ethylene glycol saturation.

Li-saturation allows identifying the charge localization between octahedral and tetrahedral sheets. In dioctahedral swelling clays, vacancies might exist in the octahedral or tetrahedral sheet. Lithium cations are able to occupy octahedral vacancies, thereby decreasing the clay permanent charge, but not tetrahedral sites. Then glycerol saturation will not induce swelling of smectitic clays with octahedral charge treated with Li but clays with tetrahedral charge will not be affected. Therefore, this saturation allows to distinguish beidellite, having mainly tetrahedral charge (> 50% of total charge), which will swell at about 17.6Å, from montmorillonite, having mainly octahedral charge (< 50% tetrahedral charge), which will collapse to 9.8 Å after Li-saturation and glycerol treatment.

The Cs-saturation procedure is a new test under development, which will is used in comparison to Li saturation. Li-saturation is not always reproducible because of dispersion problems caused by collapsed clays after heating. Comparison between the two methods will allow estimation of the layer charge and the charge localization (tetrahedral vs octahedral) of smectites.

X-ray diffraction

The device used is a D8 Advance Diffractometer of BrukerAXS company with Cu x-ray tube and LynxEye detector with Ni-filter. The program chosen was 4-70°2θ with scanning step 0.02° and 0.4 seconds per step for bulk fraction randomly oriented powder analysis. Oriented slides were scanned with X-rays from 2 to 35°2θ with a step of 0.02° and 0.3 seconds per step.

c) Glass-beads preparation for X-ray fluorescence (XRF) analysis.

About 3 g of sample were weighted, ground and placed into a previously weighted porcelain cup. The cup containing the sample was dried at 100°C for 2h, and then it was weighted to determine the dry weight. Subsequently, it was heated at 1050°C for 2h and was weighted again. The loss of ignition (LOI) of the sample is calculated from the following equation:

$$LOI = [\, [W_{\text{dried initial sample}} + W_{\text{porcelain cup}} - (W_{\text{sample after ignition}} + W_{\text{porcelain cup after ignition}}) \,] \, / \, W_{\text{dried initial sample}}] * 100$$

1.5g of ignited sample was weighted and ground in an agate mortar with 7.5g flux consisting of 50% Lithium Tetraborate – 50% Lithium Metaborate powder. The powder was homogenised, put in a Pt-crucible with 4 droplets of LiCl solution and heated to fusion for 20 min. Then the glass bead was cooled in a Pt-plate for 3 minutes and stored in desiccator for XRF analysis.

d) KBr pellet preparation for FTIR analyses

Infrared analysis was performed with KBr pellets. To prepare them, 1.5mg of the dried clay fraction were weighted and carefully ground and homogenised with 150mg of KBr. The powder was then put

into the press-holder and pressed at 10 tonnes to make a pellet. The pellet was inspected to be homogenous and placed at 150°C oven for 16h. A blank pellet was prepared consisting of 150mg of KBr, following the same procedure.

e) Cation Exchange Capacity (CEC) measurements

- *Sample preparation*

This procedure is performed for wet and for dried samples. In case of dried samples, 1.2g was heated at 100°C for at least 2h. For each sample (dry and wet), two CEC measurements were carried out.

For each sample, 0.5g were weighted and transferred into a centrifuge tube. 10mL of ammonium acetate 1mol/L were added and the suspension was stirred for 10s in ultrasonic probe and the sample was allowed to stand for 20 min. It was then centrifuged (7500 rpm, 7 min), the supernatant was decanted and 10 mL of ammonium acetate were added again. The suspension was stirred again for 10 s and allowed to stay overnight (or at least, 8h).

Because REMA sample contains Zeolites (Clinoptilolite), saturation procedure has to be done 8 times. Each time, the sample was centrifuged, the supernatant was removed and 10mL of ammonium acetate were added. The suspension was stirred for 10s and stayed overnight or at least 8h.

NH_4-saturation of sample S2 sample lasted overnight.

After finalisation of saturation, the suspension was centrifuged, the supernatant was discarded and the sample was washed 5 times with alcohol (methanol, ethyl alcohol, or isopropanol) to remove excess ammonium ions. After washing, water was added, the sample was stirred for 10s with ultrasonic probe and was transferred to the Kjeldahl microsteam apparatus.

- *Kjeldahl Microdistillation*

Connections of Kjeldahl's apparatus were greased carefully. 25mL of 1M Boric acid were transferred in a conical flask and 5 drops of bromocresol green and 2 drops of methyl red indicators were added. The colour of the solution was purple-red. The sample was placed into a 3 neck-flack and excess 5N NaOH (about 30mL) were added. Na replaced NH_4 ions, which were distilled off as ammonia and were collected in the boric acid solution through the condenser of apparatus.

When the first droplet of ammonia arrived in the boric acid solution, the colour changed from purple-red to blue-green. Distillation was allowed for 25-30min. Then heater was switched off and the conical flask with ammonia was removed.

- *Titration of the ammonia in boric acid solution*

The boric acid solution, which contained ammonia was titrated with 0.05M sulfuric acid solution using a 25mL or 50mL burette. The starting volume of sulfuric acid was quoted. Sulfuric acid was slowly added to the boric acid solution containing ammonia. End point is reached when the blue-green solution turns to buff (yellowish-beige colour). To be sure of the end point, another droplet of sulfuric acid was added. The colour turns to purple-red again. The final volume was quoted and the difference between the starting and final sulfuric acid volumes is the volume necessary to neutralise the ammonia.

CEC is calculated from the following formula:

CEC = [(V*N)/W]*100

With CEC= Cation Exchange Capacity in meq/100g or cmol/kg

V = Volume of consumed sulfuric acid,

$$N = \text{Normality of the sulfuric acid}$$

$$W = \text{Sample weight in grams}$$

f) Thermogravimetric analyses

18.81mg of ground Rema Bentonite and 24.49mg of ground S2 bentonite were placed in the pan and were heated from 35°C to 907°C with a ramp of 1°C/min. Weight variations in function of temperature were recorded.

2) Sample preparation for microbiological investigations

a) Preparation of doped-bentonites

REMA and S2 bentonites were doped with 4 different cations: Copper, Aluminium, Boron and Silver. Concerning Aluminium and boron the following procedure was adopted:

10g of ground sample were weighted on a top-balance and placed into a 500mL polyethylene centrifuge tube containing 150mL of 0.33M (1N) of H_3BO_3 solution or 150mL or 0.17M (1N) $Al_2(SO_4)_3$ solution. The suspension was dispersed with an ultrasonic probe and left overnight (at least, 8 hours). The following day, the suspension was centrifuged, the supernatant was removed and another 150mL of 1N H_3BO_3 solution or 1N $Al_2(SO_4)_3$ solution were added and allowed to rest overnight. Subsequently, the suspension was centrifuged, the supernatant removed and the clay was dried in a 60°C oven. The dried clay was then ground and stored.

In the case of Copper and Silver: 10g of each clay was doped to 1% of their respective CEC. Consequently, 10g of clay were weighted, put into a plastic beaker with 150mL of 1% CEC_{REMA} (1.9×10^{-3} mol/L for $Cu(NO_3)_2$ and 6.67×10^{-3} mol/L for $AgNO_3$) or 1% CEC_{S2} (2.0×10^{-3} mol/L for $Cu(NO_3)_2$ and 4.1 mol/L for $AgNO_3$) respectively. The suspension was stirred in the ultrasonic probe and stored for 7 days into a cupboard to avoid reaction with light, especially on Silver-doped solution. The suspension was then centrifuged, the supernatant was removed and the clay was dried at 60°C. The clay was then ground and stored in a dark-glass bottle into cupboard (or Aluminium foiled) to avoid light degradation.

Because this procedure is not easily feasible in industrial context and because the main doping procedure in industry is spraying doping-agent onto clays, another procedure was applied to compare between the "optimum" doping procedure by exchange and spray-doping-procedure which should not allow complete ion exchange. This was done only for copper and silver cations because Al and B are not submitted to ion exchange but remain in the pore solution.

For the spray-procedure, 6mL of 1% CEC_{REMA} (or CEC_{S2}) were prepared for each cation and were directly sprayed on 4g of bentonite sample without prior sieving or crushing. Samples were then dried at 60°C.

For each doped-bentonite a random powder sample for XRD was prepared and analysed.

b) Leachate preparation for MIC measurements

1600mg of each doped sample were carefully weighted and 4mL of sterilised distilled water were added to obtain 400mg/mL concentration suspensions. The suspensions were left overnight and then were checked for consistency. If suspensions were transformed to pastes, another 4mL of sterilised distilled water were added. Then all suspensions were shaken in ultrasonic bath and their consistency was checked once again. If they had been transformed to pastes, another 4mL of sterilised distilled water were added. Then the suspensions were placed in Ependorf 1.5mL tubes and were centrifuged for 15 min at 1400 RCF. The supernatant, which is the needed leachate, was then collected in new Ependorf tubes and was stored.

Table 1 gives final leachate concentration for doped-samples with their attributed number:

Tableau 1: Resume of samples number and their leachate concentrations.

Sample	Attributed number	Leachate concentration (mg/mL)
Rema φ	1	200
Rema Ag exchanged	2	400
Rema Cu exchanged	3	400
Rema B	4	400
Rema Al	5	400
S2 φ	6	400
S2 Ag exchanged	7	200
S2 Cu exchanged	8	133.3
S2 B	9	133.3
S2 Al	10	133.3

c) Minimum Inhibitory Concentration (MIC) Measurements

d) Four different microorganisms were used to determine MIC on each samples: *Staphylococcus aureus*, *Pseudomonas aeruginosa*, *Escherichia coli and Klebsiella pneumoniae.* Table 2 lists the main characteristics of these microorganisms:

Tableau 2: Studied microorganisms and their main characteristics

Microorganism	Gramm	Urease	Metabolism
S. aureus	+	+	facultative anaerobic
P. aeruginosa	-	+	strictly aerobic
E. coli	-	-	facultative aerobic
K. pneumoniae	-	+	facultative anaerobic

Each microorganism was cultivated on nutrient media overnight in an incubator at37°C to prepare inoculum solution. Some colonies were sampled from cultivation plates and mixed into LB broth media. Concentration was checked by optical density at 600nm in UVvis spectrophotometer UV mini 1240from Shimadzu Company. Optical density measurement has to be equal to 0.1 which corresponds to a concentration of 10^8 CFUs/mL in the tube. Then 1mL of 10^8CFUs/mL solution was pumped and mixed into 9 mL of LB broth media to prepare 10^7 CFUs/mL solution. This was the inoculum.

MIC and MBC were measured in 12*8 wells microplates. An example for one sample is given in Figure 2. Using 5 µL of 10^7CFUs/mL solution into 100µL well allows reaching desired concentration of 10^5CFUs/mL in each well.

Sample 2 (100 µL) +LB broth (100 µL) + microorganism	S. aureus	S. aureus	P. aeruginosa	P. aeruginosa	E. coli	E. coli	K. pneumoniae	K. pneumoniae	None	LB Broth + S. aureus	LB Broth + E. coli	LB broth
Concentration of sample (mg/mL)	200	200	200	200	200	200	200	200	200	LB Broth + S. aureus	LB Broth + E. coli	LB broth
Concentration of sample (mg/mL)	100	100	100	100	100	100	100	100	100	LB Broth + S. aureus	LB Broth + E. coli	LB broth
Concentration of sample (mg/mL)	50	50	50	50	50	50	50	50	50	LB broth	LB broth	LB broth
Concentration of sample (mg/mL)	25	25	25	25	25	25	25	25	25	LB broth	LB broth	LB broth
Concentration of sample (mg/mL)	12.5	12.5	12.5	12.5	12.5	12.5	12.5	12.5	12.5	LB broth	LB broth	LB broth
Concentration of sample (mg/mL)	6.25	6.25	6.25	6.25	6.25	6.25	6.25	6.25	6.25	LB broth + P. aeruginosa	LB broth + K. pneumoniae	LB broth
Concentration of sample (mg/mL)	3.13	3.13	3.13	3.13	3.13	3.13	3.13	3.13	3.13	LB broth + P. aeruginosa	LB broth + K. pneumoniae	LB broth
Concentration of sample (mg/mL)	1.60	1.60	1.60	1.60	1.60	1.60	1.60	1.60	1.60	LB broth + P. aeruginosa	LB broth + K. pneumoniae	LB broth

Figure 2: Representation of 12*8 wells microplates and content of each well.

After 18h to 20h incubation at 37°C, plate was placed in microplate-reader photometer, shaken and optical densities were measured at 630nm and 540nm. A mean between obtained measurements at each wavelength was calculated to obtain a value which corresponds to 585nm measurements. This wavelength was near enough to 600nm to allow reliability with inoculum optic density measurements.

e) Light effect on antibacterial properties of silver

Cat litters are not stored in perfect dark conditions, and might stay in litter house for one month. During this period, light-induced reduction of silver cations to silver nanoparticles occurs. Consequently, test the antibacterial properties evolution with light exposure is important to predict cat-litter efficiency over time. Actually, silver cation reduction to silver metal is expected to decrease silver bioavailability. But light also enhances generation of Reactive Oxygen Species (photo-Fenton Reactions, oxidations among other) which are highly effective against bacteriae and silver nanoparticles show strong antibacterial properties and low toxicity to human dermal fibroblasts (Chowdury et al., 2016). In order to have an idea of light effect, leachate was prepared with same protocol. It was stored at room light and MIC/MBC 12*8 wells plate were prepared exactly like in previous part for 1st light day, 2nd light day, 3rd light day and 7th light day (hereby, denoted as Ag-1D, Ag-2D, Ag-3D and Ag-7D respectively) . Same protocols of incubation, mixing and photometry were followed.

Results and interpretation

1) Characterisation of Rema and S2 natural samples

a) X-ray diffraction results

i) *Composition of natural samples*

Eleven phases were identified on the randomly ordered powder XRD pattern of the REMA sample with EVA software: Clinoptilolite, Smectite, Sanidine, Quartz, Albite, Anatase, Calcite, Gypsum, Pyrite, $2M_1$ Muscovite and a silica phase which could be Opal-C, Opal-CT, Cristoballite or Tridymite.

The main maxima reflexion of the silica phase is at 4.07 Å, which is between Cristobalite (101) and Tridymite (404). It suggests a mixed layer phase constituted of Cristobalite and Tridymite intergrowths (Elzea et al. 1996, Elzea et al, 1994). In addition, 2 low intensities broad peaks at 2.49Å and 2.5Å associated to a single small reflection at 4.25Å were noticeable and regarding volcanic origin of the Rema bentonite, this silica phase belongs to Opal-CT group (Elzea et al. 1994).

Quantificative determinations were obtained with the Autoquan software, and some adjustments had to be done prior to measurements. Because high sanidine does not exist in Autoquan database, Sanidine Na 0.07 was chosen because of its low content of sodium and, consequently, its high content in potassium. Opal-CT is a special phase containing poorly ordered tridymite and poorly ordered Cristobalite. To modelise Opal-CT with Autoquan, even if it is a unique phase in reality, 2 phases (Tridymite low and Cristobalite low) were used. For Smectite, because the hydration state cannot be known it was modelised with Smectite 1w (containing 1 water layer in the interlayer) and Smectite 2w (containing 2 water layers in the interlayer). A 5 degree polynomial background was selected to avoid Smectite overestimation.
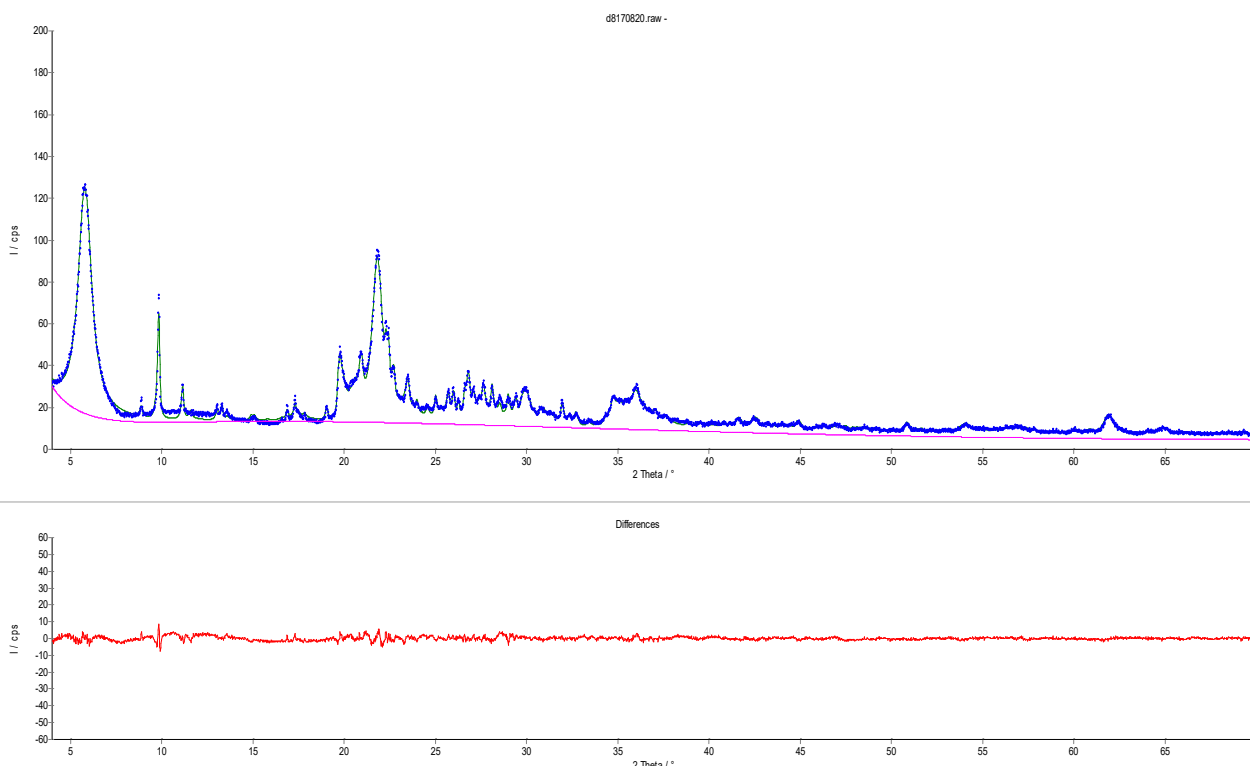
Figure 3: Rema bulk power modelised XRD pattern (up) and difference between calculated and experimental patterns (down)

The modelisation, with Rietveld refinement obtained with the Autoquan program, yielded Rwp=6.07%, indicating that profile simulation is of good qualitiy. Fitting is pretty good and some differences are noticeable mainly for clinoptilolite (intensity) and the Opal-CT region. This last one can be explained because of the use of 2 different phases for the modelisation. Clinoptilolite forms solid solution with heulandite, another zeolite mineral, and commonly exist in sedimentary rocks of volcanic origin. The difference between calculated and measured patterns may be explained considering that the structural formula of the zeolite present is intermediate between Clinoptilolite and Heulandite. Furthermore, this misfit suggests an error in Clinoptilolite calculated proportions.
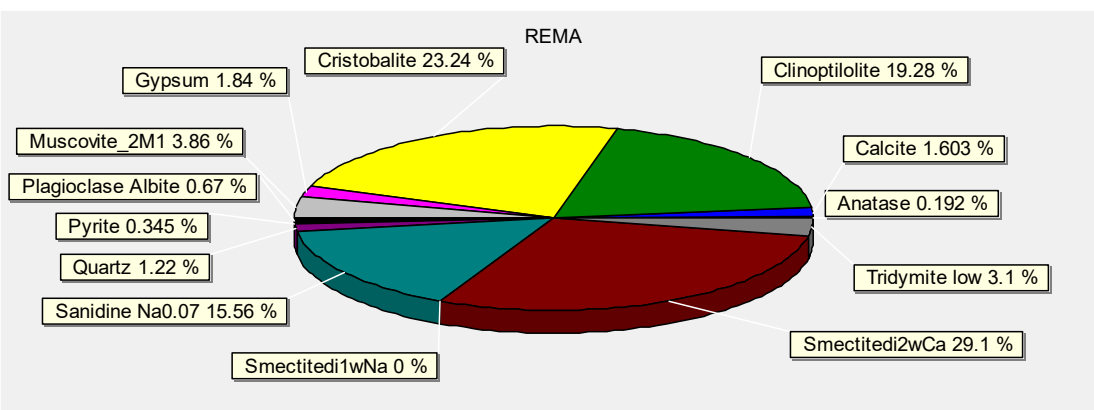
Figure 4: Calculated proportions of each phase identified in Rema

The mineralogical composition of the REMA sample is listed in Figure 4. The main phases are: Clinoptilolite (19.3%), Sanidine (15.6%), Opal-CT (26.3%), and Smectite (29.1%). Relative error of each phase (R_{phase}) was below 10%.

Considering this smectite composition, REMA is a poor quality beidellite. The presence of muscovite is surprising because of the volcanic origin of the sample, but considering it was formed from an explosive eruption, muscovite probably comes from the basement metamorphic rocks.

Table 3: Estimated proportions and relative errors for each phase present in S2

Phase	Content (%)	Relative error (%)
Anatase	0.5	0.26
Calcite	1.6	0.66
Cristobalite, defect	12.3	3.00
Gypsum	3.5	7.50
Plagioclase Andesine An50C-1	2.7	0.84
Plagioclase Labradorite An65	1.6	0.87
Pyrite	0.3	0.24
Quartz	2.5	0.42
Smectitedi1wNa	24.3	4.80
Smectitedi2wCa	46.8	5.40
Tridymite low	3.8	0.87

Eva analysis on S2 bulk randomly oriented powder pattern yielded 9 different phases: Anatase, Calcite, Opal-CT, Gypsum, Andesine, Labradorite, Pyrite, Quartz and Smectite. Similar to the Rema Bentonite, Opal-CT was distinguished from Cristobalite and Tridymite in 2 different phases and from Opal-C. (S.

Hillier et al, 2008, Elzea et al, 1994, Elzea et al, 1996, Guthrie et al, 1995, Miles et al 1994 and Ona et al 2007).
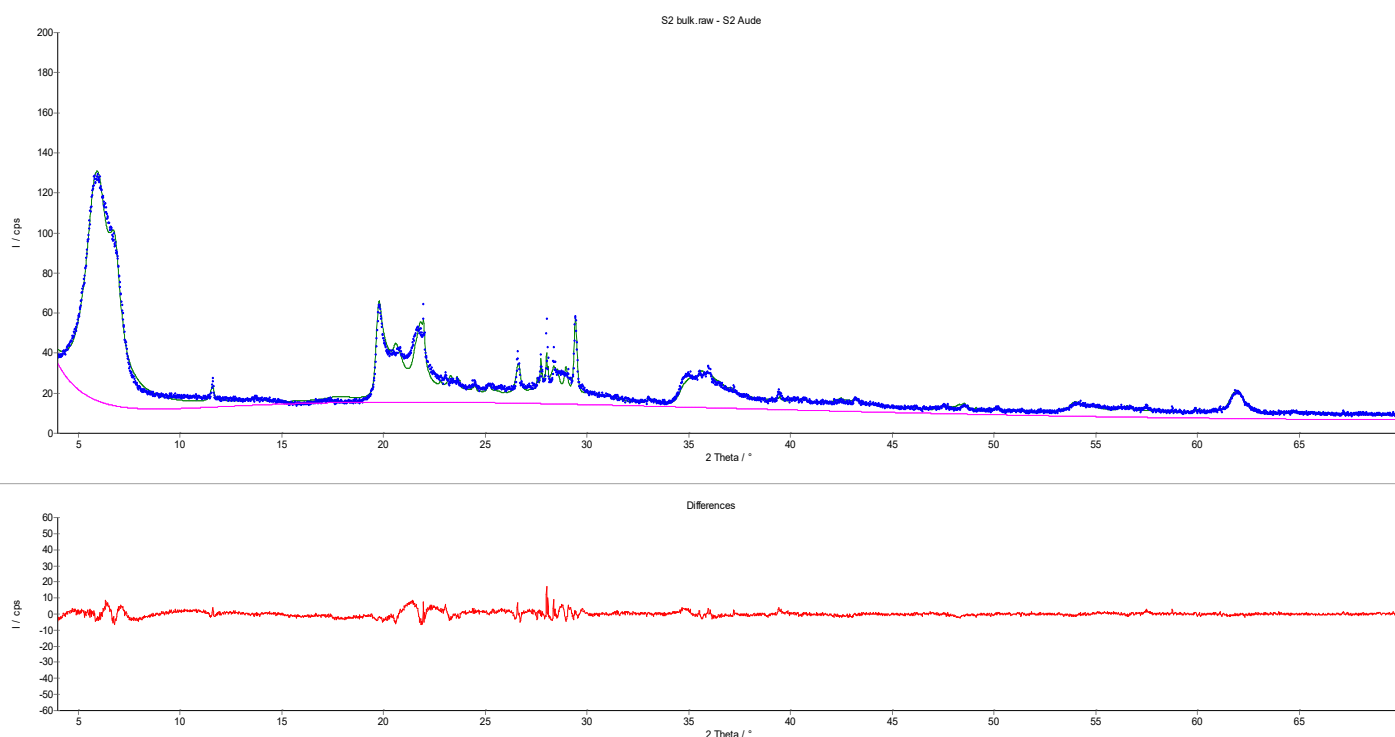

Figure 5: Bulk fraction XRD pattern and its fitting with autoquan (up) and difference between calculated and measured XRD patterns for S2

Similar to the Rema bentonite, phase adjustment had to be done for Autoquan quantification. Opal-CT was modelised with Cristobalite and Tridymite low and Smectite by Smectite with 1 water layer and Smectite with 2 water layers. Modelisation reaches Rwp=6.83% and fitting is quite good except in Opal-CT region, which can be explained by the use of 2 different phases and for plagioclase intensities. Low but existing difference was noticeable in smectite fitting, which is explained by the existence or transitionary layers containing with variable degree of hydration in the interlayer.

Calculated proportion of each phase and their relative error are reported in Table 3. The main phase is smectite (71.1%), followed by Opal-CT (16.1%). Considering this smectite composition, S2 is a good quality Bentonite.

ii)   Estimation of Smectite layer charge and assumptions concerning rheological properties

Results obtained from K-saturated EG slides were similar for both samples (figure 6). The constant layer charge concept was assumed here (Christidis et al. 2013, Tettenhorst & Johns, 1966; Cicel & Machajdik, 1981; Machajdik & Cicel, 1981). Smectite (001) main peak d-spacing was 17.02 Å in Rema and at 17.08 Å in S2 and well defined rational higher order basal reflections were observed. According to Christidis et al, 2006 and Christidis et al, 2013, both bentonites contain low charge smectites, with a layer charge between -0.30 and -0.425 per half unit cell (phuc). The smectite phase belongs to group 1a of low charge smectites. (001) Smectite peak is very asymmetric in the S2 clay fraction and not perfectly symmetric in Rema clay fraction. Consequently, smectite phase of both sample is composed of low layer charge smectite with a low proportion of layers with higher charge, belonging to group 1b of low charge Smectites (layer charge comprised between -0.425 and -0.47).

Subsequently, assumptions concerning their rheological properties are possible: Both are low charge smectites, suggesting high free swelling index (between 200 and 300 mL gel/10g of clay), viscosity and gel-strength (Christidis et al, 2006). In practice, S2 developed higher viscosity and gel-strength (gel appears at lower concentration than for Rema). This observation suggests its smectite phase has lower charge than Rema smectite phase. This is coherent with higher (001) d-spacing obtained with the K-saturated EG S2 glass slide. Another explanation for these different behaviours is the Opal-CT content difference between Rema Bentonite and S2 Bentonite. Rema bentonite contains twice as much as Opal-CT than S2 bentonite, which suggests higher quantity of clay-sized Opal-CT. This clay-sized Opal-CT are known for disturbing gel formation (Christidis et al., 2006).
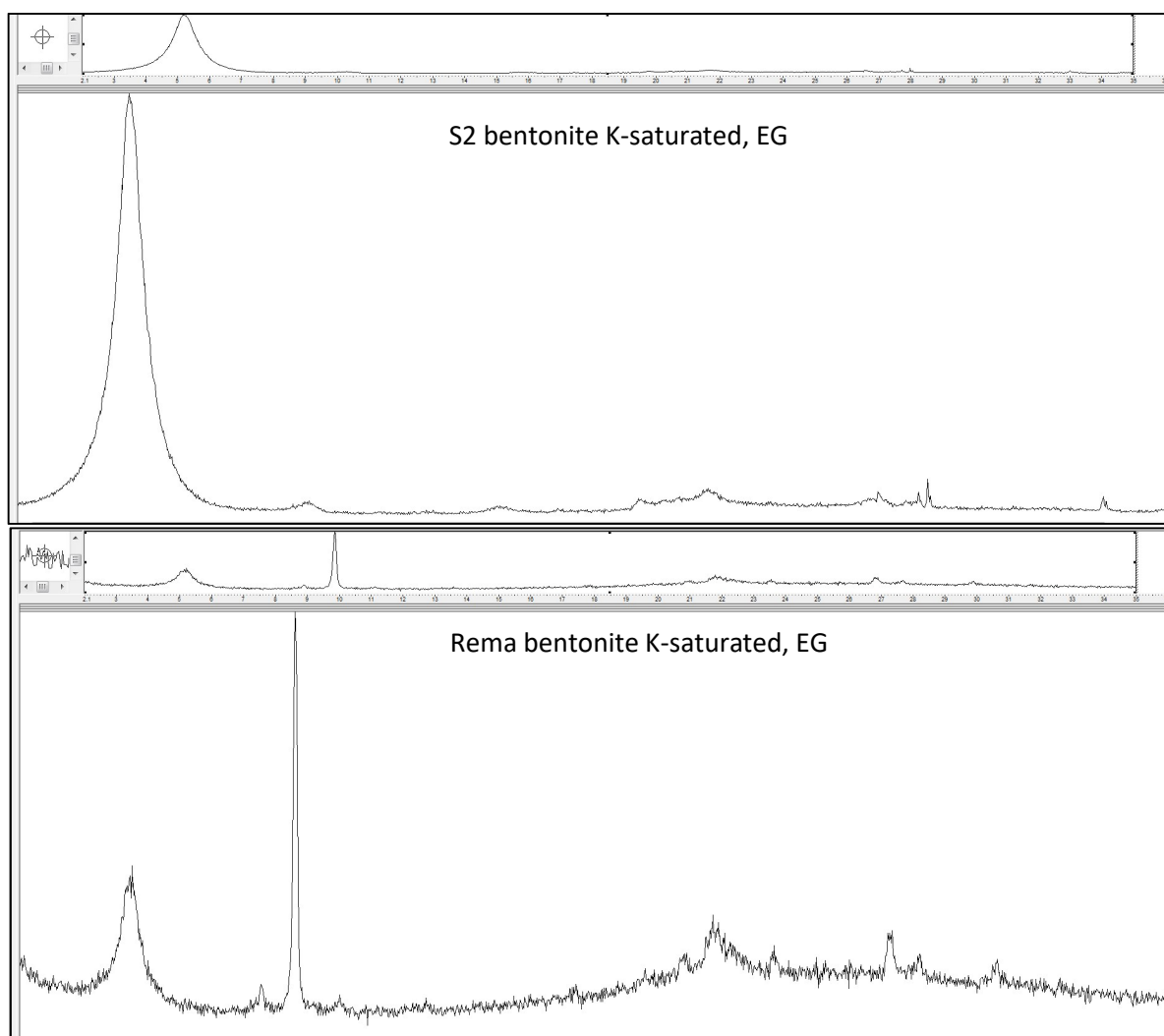
Figure 6: S2 and Rema K-saturated and ethylene glycol solvated clay fraction XRD patterns.

Li-saturation procedure allows discriminating octahedral and tetrahedral charge in samples as observed in Figure 7:
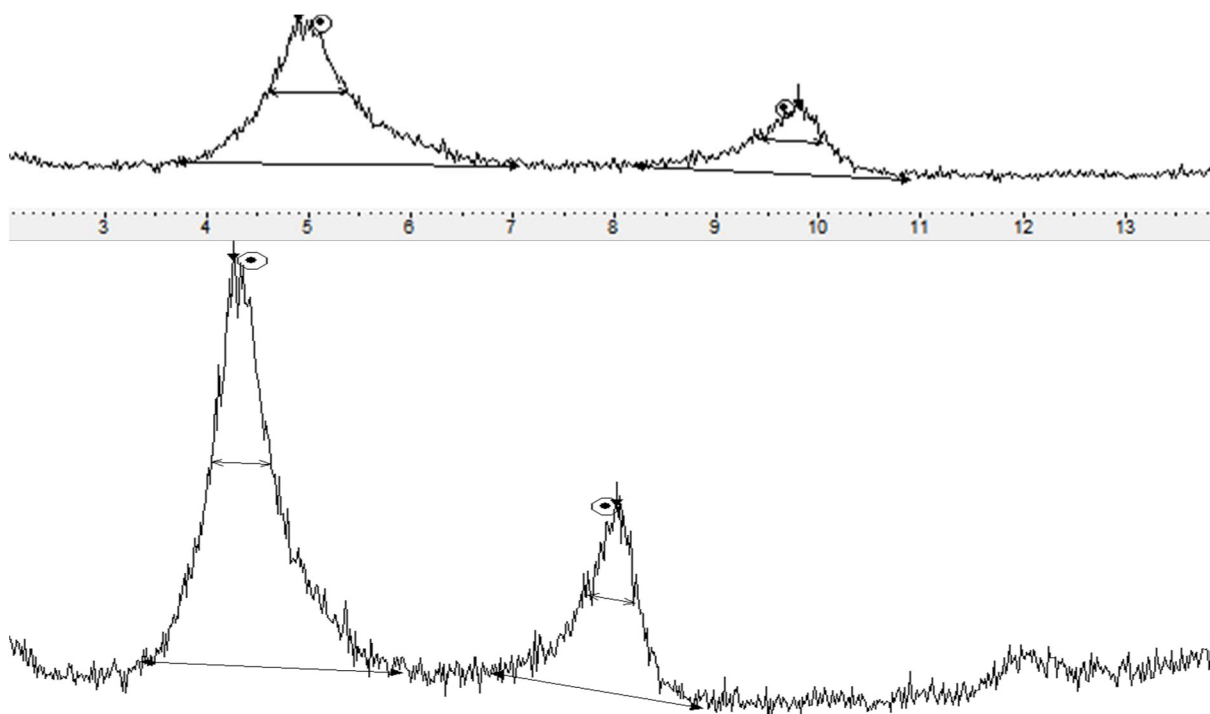
Figure 7 XRD pattern of Li-saturated S2 sample after Glycerol saturation during an overnight

In S2 bentonite, the ratio between the area below the 17.27Å peak and the area below the 9.15Å peak gives an octahedral charge percentage of 34.6%, meaning Smectite fraction is mainly composed by Beidellite. Concerning rheological properties, this bentonite has probably high plastic viscosity (Christidis et al., 2006).
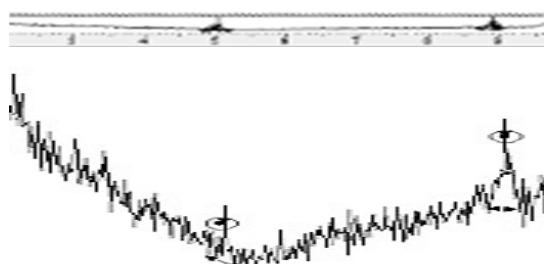
Figure 8: Best XRD pattern of Li-saturated Rema clay fraction.

Rema bentonite Li-saturated clay phase dispersion was a lot more complicated, suggesting more octahedral charge was compensated inducing more collapsed smectites. All X-ray patterns were noisy and peaks used to calculate charge distribution were not well defined or not intense (Figure 8). Consequently, a mean octahedral charge percentage was calculated with the three better XRD patterns obtained. Following similar calculation procedure, Rema smectite has an octahedral charge percentage of 59%, meaning Smectite phase is mainly composed of Montmorillonite which is coherent with dispersion problems and technical complexity during preparation of reliable XRD patterns.

Rema-Comparison between 6h and 20h Cs saturation

Rema <2 Cs - File: d8170350.raw - Type: 2Th/Th locked - Start: 2.000 ° - End: 35.009 ° - Step: 0.019 ° - Step time: 47.7 s - Temp.: 25 °C (Room) - Time Started: 21 s - 2-Theta: 2.000 ° - Theta: 1.000 ° - Chi: 0.00 ° - Phi: 0.00 ° - X: Operations: Y Scale Add 85 | Import
Rema Cs <2 6h Gly - File: d8170409.raw - Type: 2Th/Th locked - Start: 2.000 ° - End: 35.009 ° - Step: 0.019 ° - Step time: 47.7 s - Temp.: 25 °C (Room) - Time Started: 25 s - 2-Theta: 2.000 ° - Theta: 1.000 ° - Chi: 0.00 ° - Phi: 0.0 Operations: Import

S2-Comparison between 6h and 20h of Cs saturation.

S2 Cs <2 6h Gly - File: d8170410.raw - Type: 2Th/Th locked - Start: 2.000 ° - End: 35.009 ° - Step: 0.019 ° - Step time: 47.7 s - Temp.: 25 °C (Room) - Time Started: 21 s - 2-Theta: 2.000 ° - Theta: 1.000 ° - Chi: 0.00 ° - Phi: 0.00 ° - Operations: Import
Cs S2 <2 Glycerol - File: S2 Clay Cs gly.raw - Type: 2Th/Th locked - Start: 2.000 ° - End: 35.009 ° - Step: 0.019 ° - Step time: 47.7 s - Temp.: 25 °C (Room) - Time Started: 22 s - 2-Theta: 2.000 ° - Theta: 1.000 ° - Chi: 0.00 ° - Phi: Operations: Y Scale Add 85 | Import

Figure 9: Kinetic of Cs-saturation in Rema Bentonite and S2 Bentonite

Glycerol saturation of Cs saturated Rema clay fraction was completed in 6 hours. XRD patterns are similar between 6 hours of glycerol saturation and 20 hours of glycerol saturation.

Glycerol saturation of Cs-saturated S2 clay fraction is time dependent. As observed in figure 9, after 6 hours of saturation, smectite layers were not totally expanded ((001) Smectite peak occurs at lower d-spacing after 6 hours glycerol solvation than for 20 hours glycerol solvation).

In both Rema and S2 bentonite clay fractions, fully glycerol-saturated layers show larger d-spacing than natural or K-saturated Smectite. It is due to the very large atomic radius of Cesium, even compared to K (r_{Cs}=2.60 Å and r_K= 2.2Å) and not to hydration enthalpy which are in the same magnitude of order ($\Delta_r H_h^{Cs}$=-264 kJ/mol and $\Delta_r H_h^K$=-320 kJ/mol).

Furthermore, a peak at 9.98 Å appears after glycerol solvatation of Cs-saturated Smectite, which may be explain by the appearance of high charge layers due to Cesium saturation of Smectite interlayers.

S2 and Rema bentonites have similar layer charge. Consequently, the differences observed in Cesium saturation kinetic is probably due to a difference in affinity for Cesium. This difference may be due to structural differences like the octahedral charge proportion, or natural interlayer cations for which Smectite has better affinity, inducing a slower replacement in S2 smectite than in Rema smectite. Because Christidis et al, noticed evidence of a relationship between Smectite layer charge, charge

distribution and Cs-saturated (001) peak of Smectite d-spacing and because Rema smectite and S2 smectite have similar layer charge, the difference in d-spacing observed with Cs-saturated slides comes from charge distribution.

As estimated in the Li-saturated slides, S2 smectite is richer in Beidellite, and Cs-saturated (001) Smectite d-spacing is 17.62Å. Rema smectite, which is mainly composed of Montmorillonite, has (001) Smectite peak d-spacing equal to 17.56Å. These results confirm an existing relationship between Cs saturated (001) Smectite peak d-spacing and charge distribution. With only these two samples, it seems that higher the proportion of tetrahedral charge, the slower the formation of 2-layer complexes. It is also coherent with hypothesis given by Onodera et al, 1998 concerning absorption of Cesium in Smectite: An octahedral charge allows cesium to enter partially in di-trigonal cavities between tetrahedrons in the tetrahedral sheets thank to electrostatic attractions, and induces a smaller d-spacing.

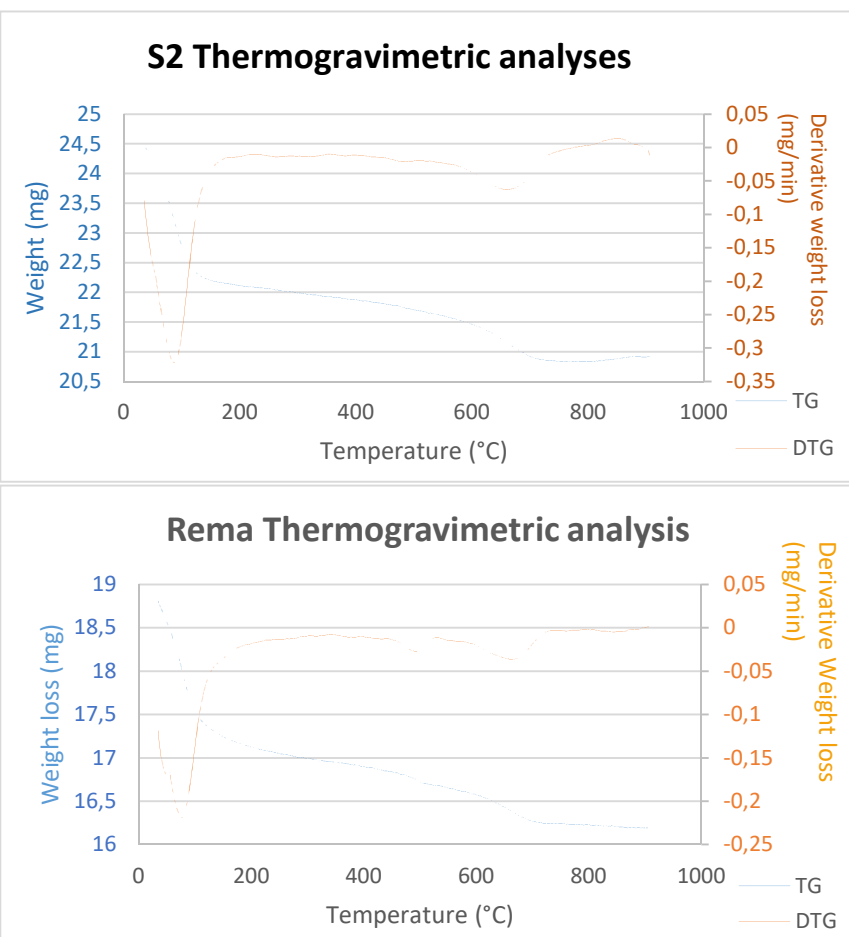### b) Clay fraction thermogravimetric analyses

Globally, thermogravimetric curves are similar for Rema and S2 bentonites. Differential curves give better precision for temperature reading. More specifically in the S2 bentonite, 3 endothermic peaks and 1 exothermic peaks was noticeable. The first weight loss of 2.36mg (9.64%) from 35 to 183°C (Derivative maximum at 87°C) corresponds to evaporation of physisorbed and interlayer water. The second weight loss of 0.77mg (3.14%) at 668°C was attributed to Smectite phase dehydroxylation. A slight gain of mass was recorded at 850°C corresponding probably to a crystallisation process. Finally the fourth weight loss of 0.03% at 880°C corresponds to calcite thermal decomposition. In addition, a constant and slow weight loss is noticeable between dehydration and dehydroxylation process corresponding probably to early dehydroxylation of nanoparticle size smectite crystals. Quartz transition from phase ɑ to phase β around 570°C was not recorded, probably because of overlapping with Smectite dehydroxylation.

Figure 10: Thermogravimetric and derivative thermogravimetric analyses measured for S2 Bentonite and Rema Bentonite.

Thermogravimetric curve of Rema Bentonite shows 4 endothermic peaks. The first weight loss of 9.06% at 79°C corresponds to evaporation of physisorbed and interlayer water from Smectite but also to gypsum water loss. The second weight loss of 0.61% is related to muscovite dehydroxylation. At 670°C, the weight loss of 1.8% corresponds to Smectite dehydroxylation (which is lower than expected from Christidis, 2008). In addition, such weight loss from smectite dehydroxylation indicates smectite content of about 40%, which supports the hypothesis of an underestimation of smectite content in

Autoquan modelisation. Finally, at 850°C, the weight loss of 0.26% was associated to calcite thermal decomposition.

In both bentonites, results given by thermogravimetric analysis are coherent with the XRD patterns. They also show evidences of Stoke's law limitations, used for clay extraction. Indeed, quartz and calcite are still present, but in low quantities compared to bulk fraction. Furthermore, the weight loss associated to an illitic phase in S2 bentonite, which was not identified in XRD patterns, may be explained with the XRD detection limits or with sample sizes used in each technics. Even if each sample fraction is globally representative of whole sample, locally some mineralogical differences may occur.

c) FTIR results: Precisions about clay characteristics and substitutions

The KBr pellets of both samples show bending and stretching bands of adsorbed water (at about 3460cm^{-1} and 1635 cm^{-1}) even after overnight drying of the samples before making the pellet and an overnight drying of the pellets afterwards. The bending band of H$_2$O (Van Der Marel et al. 1976, Madejova et al. 2011) is present in both samples (1638 cm^{-1} for Rema and 1635 cm^{-1} for S2).

Carbonate specific bending band is noticed at about 1430 cm^{-1} in Rema and S2 bentonites.

The intense band at 795cm^{-1} in Rema and S2 bentonites is typical of SiO$_2$ species (Van Der Marel et al. 1976, Madejova et al. 2011). Its important intensity is coherent with the percentage of quartz and Opal-CT (about 20% in total in both samples) obtained with Autoquan software.

The intensity ratio between OH stretching bands and Si-O stretching bands in both samples is strongly superior to 1. It is typical of 2:1 clay fraction, which is coherent with previous observations.

In both samples, the OH-bending bands are present between 800cm^{-1} and 900cm^{-1} suggesting that the smectite present is dioctahedral (Madejova et al. 2011). The different abundance of the clay fractions between Rema and S2 is also confirmed by the FTIR scans because the OH-bending bands of S2 are more intense than in Rema. Finally, the bands between 2955cm^{-1} and 2850cm^{-1} are attributed to organic compounds, probably due to contamination during preparation of KBr pellets.

More specifically in the Rema bentonite, the OH stretching bands between 3625 cm^{-1} and 3665 cm^{-1} are typical of Smectite and muscovite (Van Der Marel et al. 1976, Madejova et al. 2011). The band at 3665 cm^{-1} combined to the OH bending band at 726 cm^{-1} is typical of Al--OH in muscovite (Van Der Marel et al. 1976, Madejova et al. 2011), which is in accordance with the XRD identification of muscovite at 9.99Å.

The stretching bands at 3642 cm^{-1}, 3625 cm^{-1}, 1115-1090cm^{-1}, 1044 cm^{-1} and bending bands at 846 cm^{-1}, 884cm^{-1}, 920 cm^{-1} are typical of dioctahedral montmorillonite and gives information about Fe and Mg substitution for Al in octahedra (Van Der Marel et al. 1976, Madejova et al. 2011), which is confirmed by an intense Si-O-Mg bending bands at 496cm^{-1}. These substitutions indicate octahedral charge in smectite, in accordance with the XRD results.

Bending bands observed at 727 cm^{-1}, 703 cm^{-1}, 676cm^{-1} and 619 cm^{-1} confirm Fe and Mg substitution in the clay fraction. It is probably mainly Fe substitution in octahedrons, which explains the shift of the Si-O-Al bands to 727 cm^{-1} (Van Der Marel et al. 1976, Madejova et al. 2011).

In sample S2 the OH-stretching bands at 3640 cm^{-1} and 3626 cm^{-1} combined to the bending bands between 800cm^{-1} and 900 cm^{-1} are typical of montmorillonite (dioctahedral smectite). Substitutions of octahedral Al by Mg and Fe are noticeable (3640 cm^{-1}: (Mg,Al)-OH stretching band, 881cm^{-1}: Al-Fe-OH bending band, 846cm^{-1}: Al-Mg-OH bending band and confirmed by the Si-O-Mg bending band at 468 cm^{-1} and at 664cm^{-1} (Van Der Marel et al. 1976, Madejova et al. 2011).
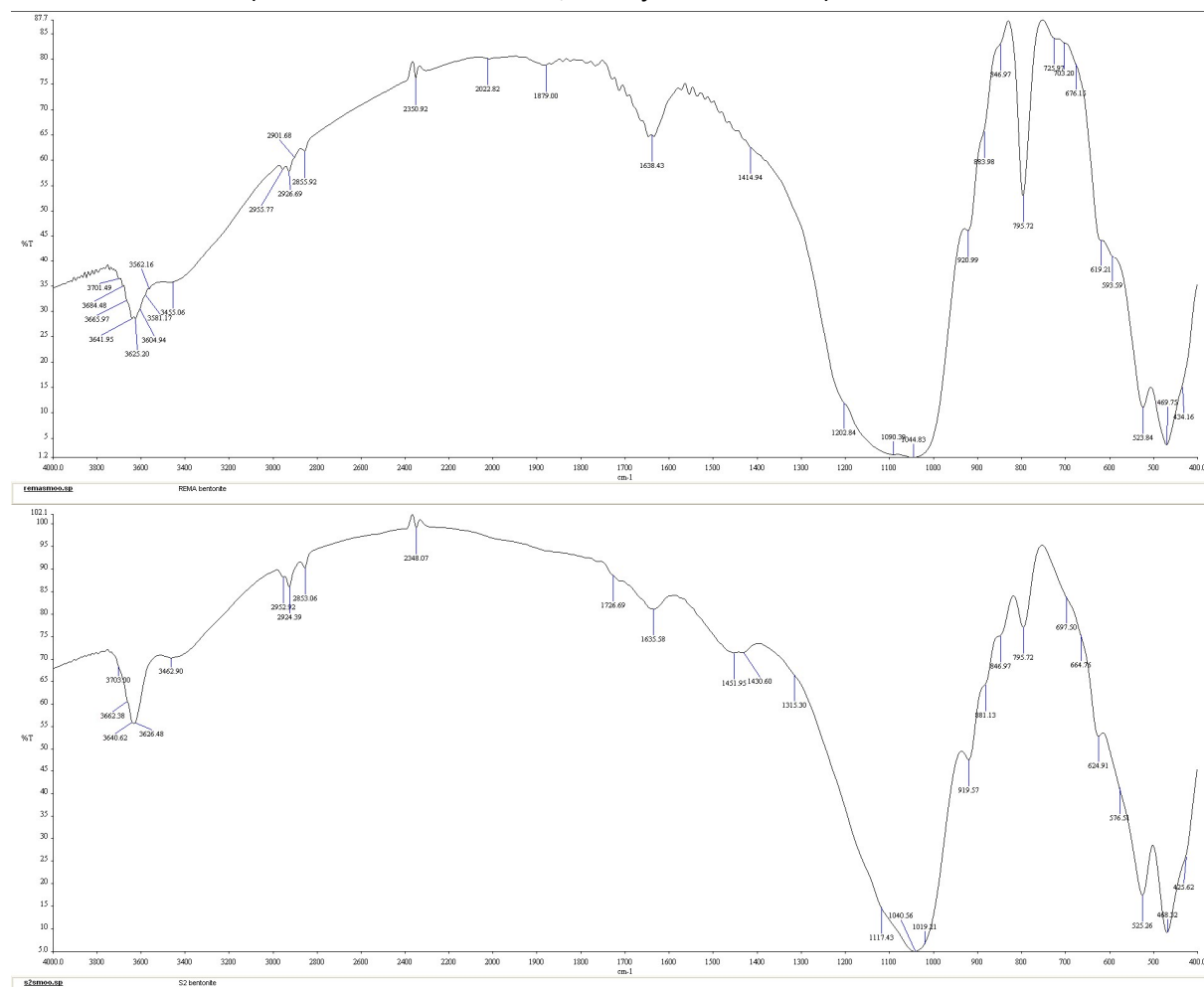
Figure 11: FTIR scans of S2 Bentonite+KBr pellet (up), and Rema bentonite + KBr pellet (low)

d) XRF results: Water loss, Loss on Ignition and structural formulas of smectites

Table 4: Water loss and Loss on Ignition of Rema bentonite and S2 bentonite

Sample	Initial Weight (g)	Weight after 100°C, 2h (g)	Weight after 1050°C, 2h (g)	Water Loss (%)	Loss of Ignition (%)
Rema	3.2475	3.0431	2.8413	6.2941	6,6314
S2	5.0475	4.4999	4.1269	10.8489	8,2891

Results obtained with XRF analysis are given in table 5:

Table 5: Oxide percentages obtained with XRF glass-beads analyses of fired samples (LOI free)

Sample	Na2O (%)	MgO (%)	K2O (%)	CaO (%)	TiO2 (%)	MnO (%)	Fe2O3 (%)	Al2O3 (%)	SiO2 (%)	P2O5 (%)	Total (%)
S2	2,34	2,88	0,57	7,46	0,52	0,05	3,78	15,89	63,05	0,17	96,71
Rema	0,58	1,43	2,44	1,42	0,34	0,02	1,83	13,23	74,99	0,01	96.29

Calcium oxide percentage is higher than expected in S2 Bentonite. It suggests pollution or local enrichment of calcium (grain richer in calcite or gypsum crushed during preparation for example). Because these results are representative of a small sample fraction, it seems appropriate to use them very carefully. A "mean" structural formula of S2 bentonite Smectite phase was calculated fwith the SF method from A. Bouchet et al. 2000. Considering calcium, because of high measured percentage, it was only used to balance layer charge. S2 smectite calculated structural formula is:

$(Si_{3.97}Al_{0.03}) O_{10} (Al_{1.14}Fe^{III}_{0.18}Mg_{0.27}Ti_{0.04}) (OH)_2 Ca_{0.02}K_{0.05}Na_{0.29}$
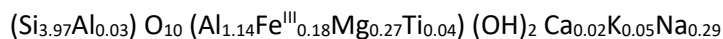
This formula is not the real one of Smectite phase in S2 bentonite. It is an average of all smectite microcrystallites present in this phase. But, it is an approach to verify datas coherence. Actually, S2 beidellite layer charge should be between -0.30 and -0.35 (K-saturated XRD pattern interpretation), and it is coherent with calculated layer charge from XRF results (-0.35). In addition, this Na-smectite is also coherent with thermogravimetric weight loss during dehydration which is inferior to 15-20%, higher possible amount expected for a Ca-smectite (Christidis, 2008). But charge distribution is not in agreement with Li-saturated pattern results. In this calculated formula, charge comes mainly from octahedral layer (more than 90%) resulting in a Montmorillonite but Li-saturated XRD pattern clearly demonstrates an octahedral layer charge percentage inferior to 50%. This error is discussed by Christidis, 2008 and can belong to SF methodology. Furthermore, this difference comes also probably from modelisation giving approximated phase percentages with phases especially adapted for this software, but can also come from XRF analyses that are only focused on some elements (for example, Fe^{2+} is missing). More reliable structural formulae could be obtained with microbeam technics allowing precise elements measurement on single crystal with low accessory minerals contamination (thank to electron beam precision). Still, alkali volatile elements and iron (II) are not determined in such analysis. Finally these results define S2 bentonite as a Na-Bentonite, which is in agreement with its good colloidal properties.

Rema bentonite structural formula cannot be calculated because of Clinoptilolite phase. This phase has a high variety of potential structural formulas and is probably not pure Clinoptilolite but a mineral phase between Clinoptilolite and Heulandite. Additional assumptions are needed compared to S2 bentonite. For example, by comparison with Clinoptilolite database, Si/Al ratio was calculated and the more comparable known Clinoptilolite was selected to represent Rema Clinoptilolite phase. In addition, it is not possible to know if Rema contains "K-Clinoptilolite", "Na-Clinoptilolite" or "Ca-Clinoptilolite" or a mix of them (probably the better choice), LOI was calculated as the mean of the LOI of these three different clinoptilolites.

These assumptions induce an overestimated Si quantity in the Smectite phase (superior to 4 per unit formula), which does not allow writing the structural formula.

Regarding CaO, K_2O and Na_2O percentages in XRF results, Smectite phase has a high quantity of K^+ in the interlayer compare to Na^+ and Ca^{2+}. It is, consequently, a "K-bentonites" which confirms, its volcanic ash origin.

e) Cation Exchange Capacity of REMA and S2 and layer charge calculation

The CEC of the samples both at room humidity and dried overnight at 105°C, were determined from several replicates and are listed in Table 6:

Table 6: Cation Exchange Capacities of Rema bentonite and S2 bentonite

Sample S2	CEC experimentally measured (meq/100g)
1	58.7
2	58.7
3	62.7
4 (Dried)	62.4
5 (Dried)	62.4
Average value	60.9
Sample REMA	CEC experimentally measured (meq/100g)
1	56.6
2	56.6
3 (Dried)	55.6
4 (Dried)	55.8
Average value	56.2

According to Autoquan modelisation, S2 smectite content is 71.1%. There is no other phase exhibiting a CEC in this sample. Normalised to 100% of Smectite, CEC of S2 smectite is 85.7 meq/100g. Rema Smectite content is 29.1%. But this sample is also composed of 19.8% of Clinoptilolite, which has a CEC about equal to 225 meq/100g in pure state giving $CEC_{clinoptilolite}$= 4.1meq/100g in Rema. In consequence, CEC really coming from Smectite corresponds to 59.6% of experimentally measured CEC. Finally measured CEC corresponding to Rema Smectite is 33.6meq/100g. In pure phase, CEC of this Smectite would be 115.5 meq/100g.

The small difference between these values can be explained by the presence of Clinoptilolite in Rema bentonite which compensates the low Smectite content. The CEC measured values are very low compared to the Smectite and Clinoptilolite content in both samples. After verification of the experimental device and because the error is systematic, an experimental error is not possible. The pH of distilled water used has been measured and is more acidic than it should be (around 4.5). This acidic pH can explain the lower CEC values and the systematic error. Because this water is used in all experiments, these values will be conserved and will be coherent with all other results depending on water acidity.

Furthermore, as discussed by Christidis 2008, CEC measured at pH=4 (not far from our experimental pH) induces the measurement of positively charged smectite edges, avoiding CEC overestimation coming from edge ability to exchange cations. In conclusion these CEC measurements are not false but are linked only to interlayer cation exchange capacity and estimate permanent CEC and layer charge.

An estimation of the layer charge of both bentonites is possible through comparison with experimental linear regression done in MRED laboratory for Kjeldhal microdistillation CEC measurements.
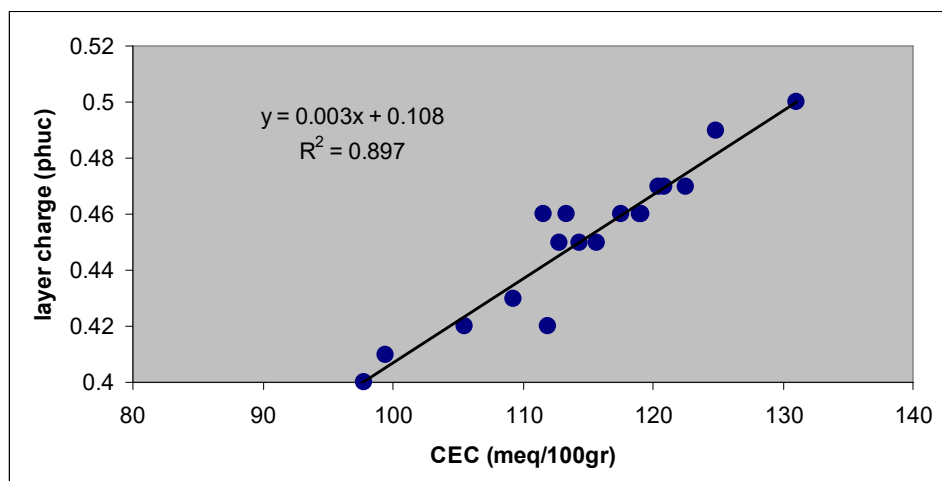
Figure 12: Layer charge estimation in function of CEC obtained with Kjeldhal microdistillation.

The estimated S2 beidellite layer charge is 0.348 phuc, which is very near to the layer charge estimated with K-saturated XRD pattern and the layer charge calculated with SF method. The estimated Rema layer charge from CEC is 0.453 phuc, which is strongly higher than estimated from XRD results. Actually, clinoptilolite is not perfectly fitted by Autoquan software, especially in term of intensity. This partial misfit suggests an overestimation of clinoptilolite content in Rema bulk powder and induce Smectite layer charge overestimation here. Once again, this difference confirms the complexity of mineralogical characterisation in samples containing more than one mineral with variable structural formula, CEC and layer charge.

2) Characteristics of doped (modified) bentonite samples

Natural Rema and "Doped" Rema XRD pattern comparison

REMA Cu - File: d8170499.raw - Type: 2Th/Th locked - Start: 4.000 ° - End: 69.998 ° - Step: 0.019 °- Step time
Operations: Y Scale Add -254 | Y Scale Add 288 | Import
REMA Aude - File: REMA bulk.raw - Type: 2Th/Th locked - Start: 4.000 ° - End: 69.998 ° - Step: 0.019 °- Step t
Operations: Y Scale Add 864 | Y Scale Add 186 | Y Scale Add 898 | Y Scale Add -661 | Y Scale Add 1000 | Imp
REMA Ag - File: d8170500.raw - Type: 2Th/Th locked - Start: 4.000 ° - End: 69.998 ° - Step: 0.019 °- Step time
Operations: Y Scale Add 525 | Y Scale Add 119 | Y Scale Add 864 | Y Scale Add -390 | X Offset 0.000 | Y Scale
REMA AP - File: d8170464.raw - Type: 2Th/Th locked - Start: 4.000 ° - End: 69.998 ° - Step: 0.019 °- Step time
Operations: Y Scale Add -220 | Y Scale Add -254 | Y Scale Add -525 | X Offset 0.000 | Y Scale Add 525 | Import

REMA B - File: d8170468.raw - Type: 2Th/Th locked - Start: 4.000 ° - End: 69.998 ° - Step: 0.019 °- Step time:
Operations: Y Scale Add 390 | Y Scale Add 390 | Y Scale Add 864 | Import

Natural S2 and "Doped" S2 XRD pattern comparison

S2 Ag - File: d8170502.raw - Type: 2Th/Th locked - Start: 4.000 °- End: 69.998 ° - Step: 0.019 °- Step time 63
Operations: Y Scale Add 797 | Import
S2 Aude - File: S2 bulk.raw - Type: 2Th/Th locked - Start: 4.000 ° - End: 69.998 ° - Step: 0.019 °- Step time 63
Operations: Y Scale Add 1000 | Y Scale Add 492 | Y Scale Add 288 | Import
S2 Cu - File: d8170501.raw - Type: 2Th/Th locked - Start: 4.000 ° - End: 69.998 ° - Step: 0.019 °- Step time 63
Operations: Y Scale Add -458 | Y Scale Add 559 | Y Scale Add 559 | Y Scale Add -322 | Import
S2 Al - File: d8170466.raw - Type: 2Th/Th locked - Start: 4.000 ° - End: 69.998 ° - Step: 0.019 °- Step time: 63.
Operations: Y Scale Add 220 | Y Scale Add 254 | Y Scale Add -797 | Import

S2 - File: d8170467.raw - Type: 2Th/Th locked - Start: 4.000 ° - End: 69.998 ° - Step: 0.019 °- Step time: 63.6 s
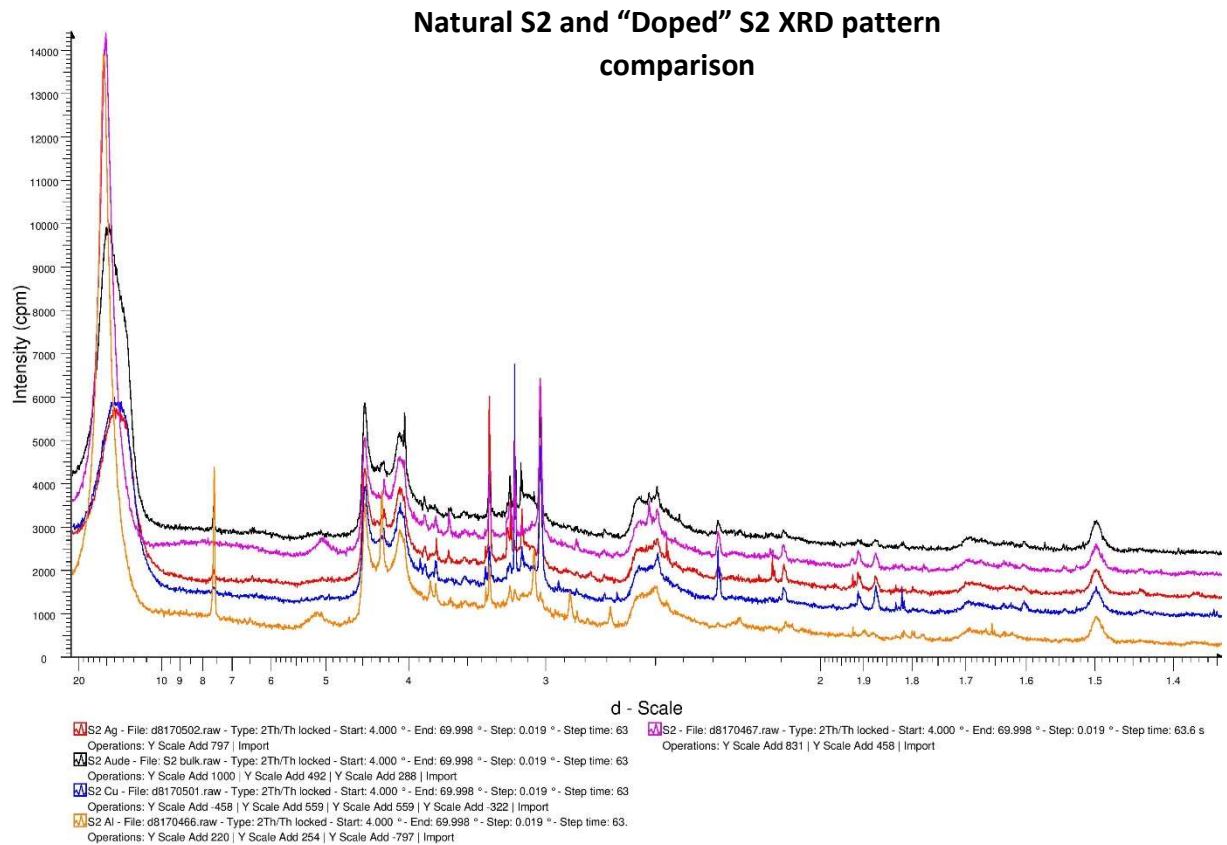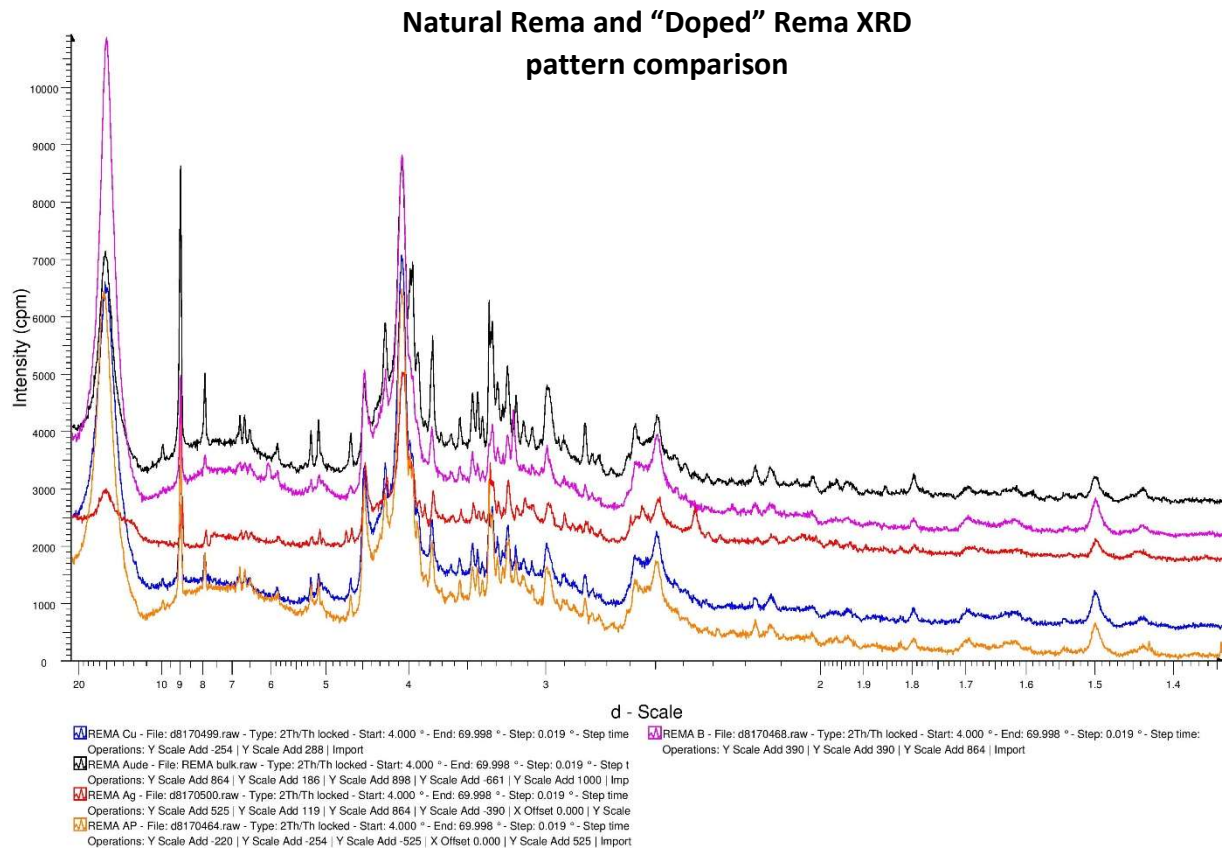Operations: Y Scale Add 831 | Y Scale Add 458 | Import

Figure 13: Comparison between Natural Rema bulk fraction XRD pattern and modified Rema bentonite XRD patterns (up).

To monitor the success of the saturation by copper, aluminium, silver and boron, XRD patterns of the doped were obtained using random powder samples. The patterns were compared to the original powder XRD patterns (figure 13). In the case of Cu and Ag saturation, a shift of the Smectite (001) diffraction maximum is noticeable because of doping. For Al-doped and B-doped bentonites, the basal d-spacings are comparable to those of their original counterparts with 2 water layers in interlayer. This behaviour is explained by the inability of Al and B to enter the interlayer, but during exchange procedure, Smectite can take water from the solution and swells to its maximum.

In the Cu-doped and Ag-doped bentonites, the d_{001}-spacing slightly decreased compared their natural counterparts. This is attributed to the smaller diameter of the hydrated Cu- and Ag-ions compared to the hydrated Ca-ions. Also, in Rema bentonite, Ag-doping yielded two basal smectite reflections, one at ~ 13Å after one week saturation, suggesting that single water layer complexes were formed, probably related to the Ag- ions and one at 15 Å indicating 2 water layer complexes. It is not surprising since saturation solutions were prepared with only 1% of the CEC in Ag^+ and Cu^{2+}. Verification is possible by the used of solution containing higher percentage of the CEC. Furthermore, the intensity of the Ag-Rema (001) peak is significantly lower. This difference, only related to the saturation with silver in Rema smectite and related to silver and copper saturation in S2 smectite, suggests a change in smectite texture. Actually, the decrease of (001) peak intensity means a smaller number of smectite crystallites oriented in parallel to (001) plane. The two smectite populations, the first with 2 water layers in interlayer and the second saturated with silver, don't have the same "thickness" in c direction because the content of their interlayer is different. Consequently, the stacking of smectite crystallites is less oriented when powder is added to the holder. In contrary, B-rema, B-S2 and Al-S2 (001) peaks have higher intensities compared to original powder. It suggests larger number of smectite crystallites with (001) orientation. Actually, all smectite interlayers reach their maximum swelling capacities, which induces homogenisation of interlayer thickness. Consequently, smectite crystallites are more oriented in the same direction when placed in sample holders. Figure 14 is a very simplified and schematic representation of these explanations.
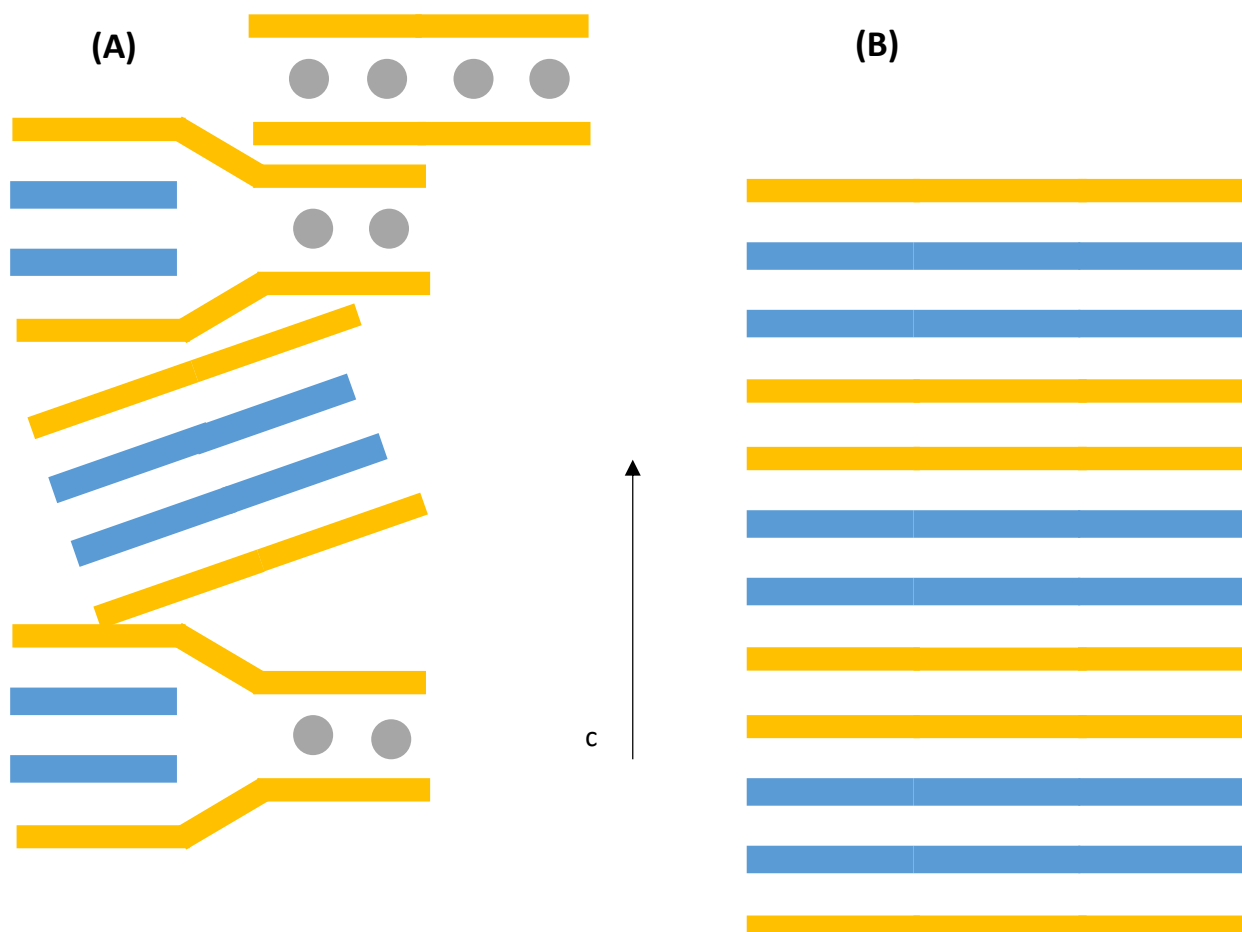
Figure 14: Simplified and schematic representation of (A) smectite stacking potential disorder with different interlayer thickness. (B) Smectite stacking order in case of identical interlayers. Yellow layers: smectites layers, Blue layers: Water layers in interlayer, Grey circles: Silver cations and their hydrated sphere in interlayer.

3) Bacteriostatic and Bactericidal properties of natural and doped bentonites

a) Natural antibacterial properties

As expected, Rema bentonite doesn't have strong antibacterial properties in its natural form. But, as observed in figure 15, this clay shows natural bacteriostatic properties, and even bactericidal properties for high leachate concentrations especially against *S. aureus*. These properties are dose-dependent but don't follow a linear tendency. Actually, concerning *E. coli* and *P. aeruginosa*, a logarithm-type dependence is observed. Concerning *S. aureus* and *K. pneumoniae*, bacteriostatic properties reach a first efficiency maximum at middle concentration (25mg/mL), then decrease to 50mg/mL and increase once again to the maximum tested concentration. Bacteriostatic effect is seen only for *S. aureus*, suggesting a gram-type dependence antibacterial effect. The leachate contains nanoclay particles, exchangeable cations, nanoparticles of pyrite and anatase.

S. aureus is the only Gram + tested bacteria, which suggests a mechanism through physical interaction between clay particles and peptidoglycan layer of this bacteria. The --OH groups of Smectite edges are probably involved in this mechanism and Rema Montmorillonite seems to have more affinity for peptidoglycans (gram + cell wall) than for gram - phospholipid outer membranes. This suggests an interaction between --NH$_2$, --OH and/or --COOH groups contained in these organic molecules and Montmorillonite. The gram + higher sensitivity may suggest that --NH$_2$ and/or --COOH are particularly involved in this physical mechanism. --OH groups also have labile protons in α position, which may
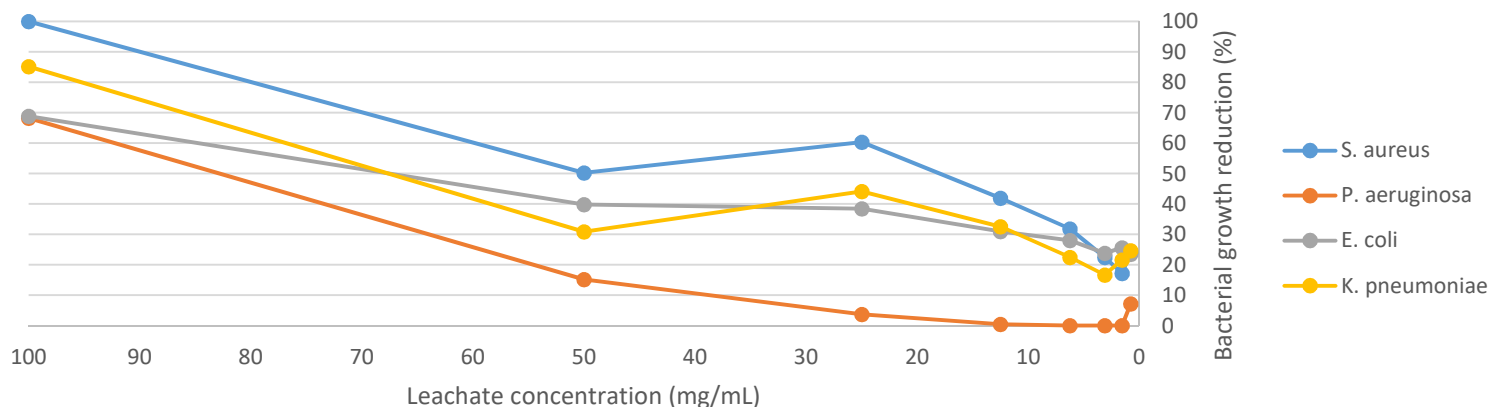
induce an acidification of bacteria environment and peptidoglycan layer disruption. Antibacterial properties are also visible on Gram - bacteriae and because of leachate composition, it is also suggested that Rema clays interlayer contains naturally an organic molecule or a cation which has moderate antibacterial properties. Another explanation is the presence of clay nanoparticles having competitive affinity for vital elements like potassium, inducing growth reduction compare to positive control.

This bacteriostatic and bactericidal effect can also be induced by TiO_2 nanoparticles, coming from anatase, and iron coming from Pyrite in leachate. Both of them have well known antibacterial properties: Titanium dioxide particles are used in waste water treatment through heterogeneous photocatalysis. Even if light (and especially UV-A) exposure is short in our case, it is able to generate some hydroxyl radicals from water and organic compounds contained in the leachate and in LB broth. This reactive oxygen specie induces an oxidative stress for bacteria, and interaction between TiO_2 nanoparticles and bacterial surface induces deformation and morphological changes, destruction of intracellular components and DNA damages resulting in bacterial death.

Pyrite is also potentially involved in these moderate bacteriostatic and bactericidal effect because of Fe importance in photo-Fenton and Fenton reactions through oxidation of Fe^{2+}, which also induce oxidative stress to bacteria and cell damages through the action of reactive oxygen species. Considering the short insolation period and low concentration of anatase and pyrite in Rema bentonite, these mechanisms are probably not strong and the observed effect is probably a combination of the different cited mechanisms.

In contrary, natural S2 bentonite has strong natural antibacterial properties towards all tested bacteriae and even at the lowest leachate concentration (2.1mg/mL). It is not even possible to get MIC50 (representing 50% of growth reduction, classically considered as "no visible growth" with eyes).
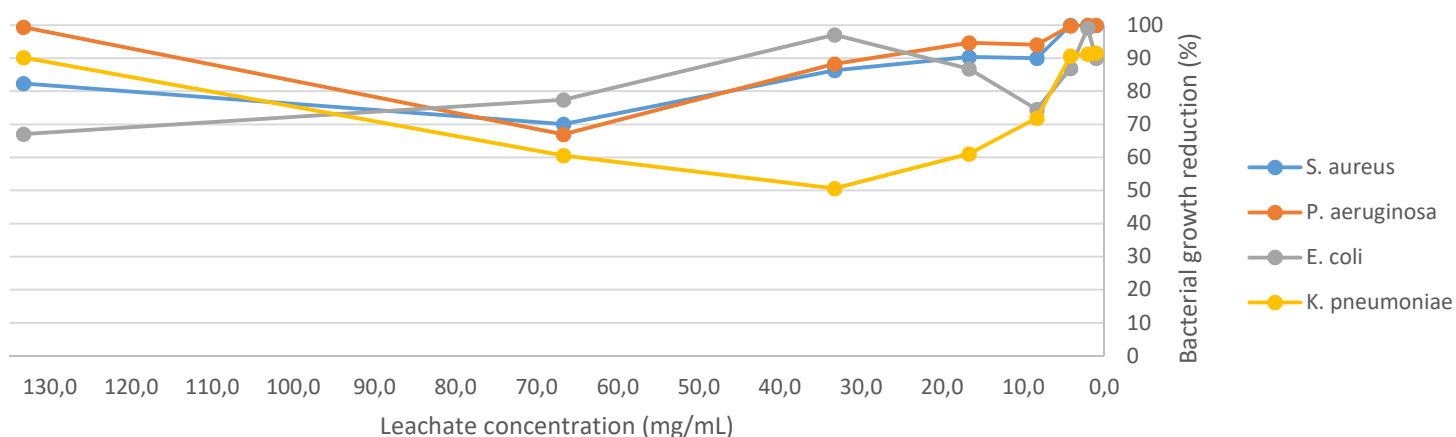

Figure 15: Rema bentonite and S2 bentonite natural antibacterial properties

Consequently, MIC90 (90% of growth reduction compared to positive control) are also defined because data are available (Figure 15). All mechanisms mentioned for Rema are probably involved in these bactericidal and bacteriostatic effects but they cannot justify this strong efficiency by itself even if S2 Beidellite content is more than twice higher than in Rema bentonite. Another assumption is the presence of organic or inorganic compounds or specific cations in interlayer that display great natural antibacterial properties. This assumption can be verified with copper and silver modified S2 bentonites, because the doping process is based on cation exchange and Ag and Cu could replace this substance potentially in interlayer.

b) Impact of doping on antibacterial properties

In all cases (except Al-S2) antibacterial properties of doped materials are dose-dependent but rarely follow a linear tendency.

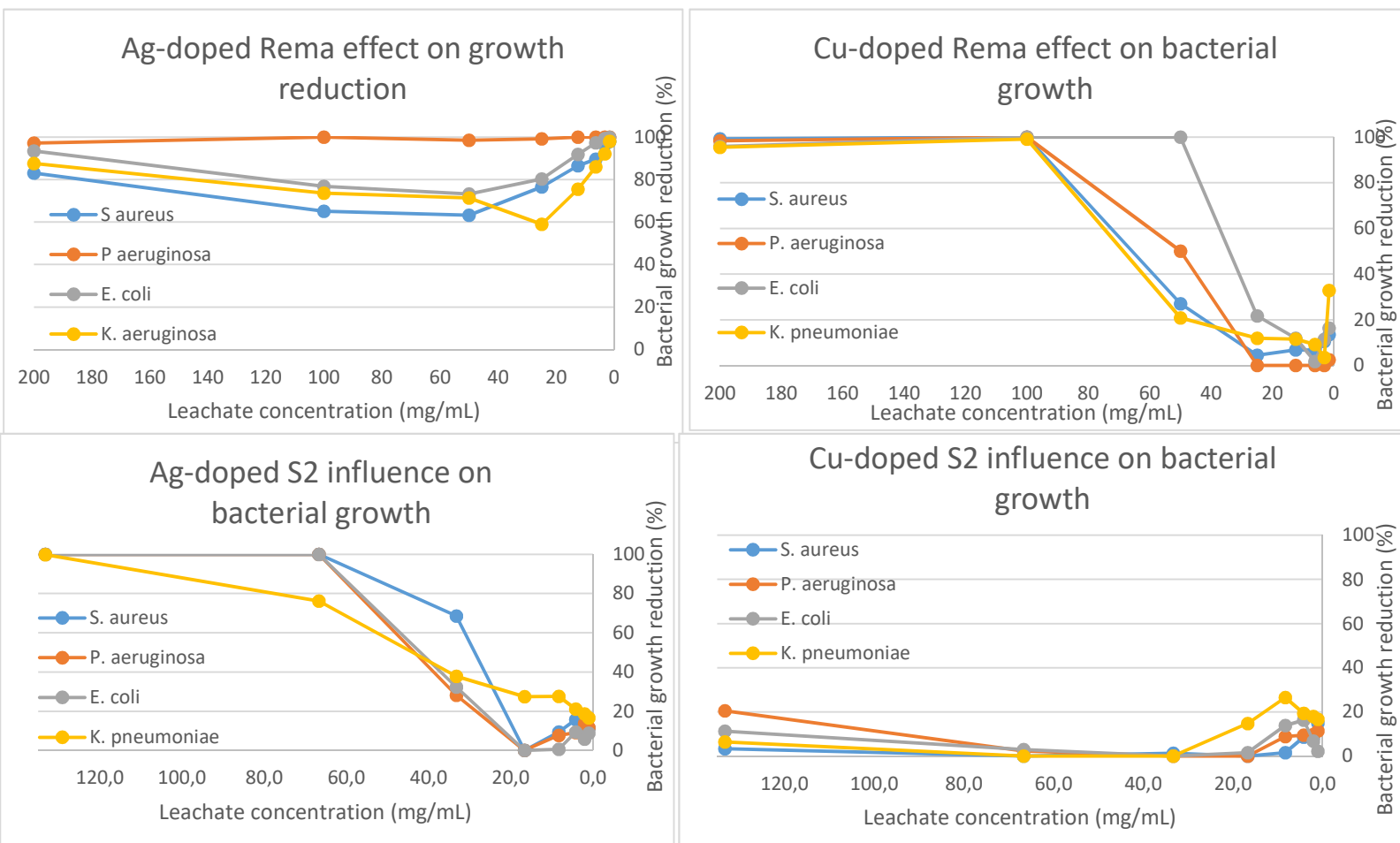*i)   Effect of copper and silver on antibacterial properties*

Figure 16: Ag- and Cu-modified bentonites effect on bacterial growth

The presence of Copper or Silver in Rema Montmorillonite interlayers induces a significant increase of antibacterial properties. Silver offers bactericidal and strong bacteriostatic properties in all tested concentrations, giving to this sample growth reduction between 60% and 100% regardless of the leachate concentration. Efficiency of this material is also stronger at lower leachate concentration, meaning that the best antibacterial effect against gram + and gram - bacteriae is obtained for low silver cation concentrations.

Concerning Cu-doped Rema bentonite, the antibacterial effect is observed only for middle and high leachate concentration. In addition, a bactericidal effect is observed against all bacteria species for leachate concentration higher than 100mg/mL and the MBC is even lower for *E. coli*.

In the S2 bentonite, silver exchange induces the loss of antibacterial properties for low leachate concentrations but confers bacteriostatic effect at high leachate concentrations (MBC=66.7 mg/mL for *E. coli, S. aureus* and *P. aeruginosa* and MBC=133.3 mg/mL for *K. pneumoniae*). Antibacterial properties are conserved but they are observable only at high concentration. Copper exchange doesn't offer antibacterial properties to this sample, even if it is known as a strong antibacterial agent in many previous studies (Zhao et al, 2006, Martucci et al, 2017, Hu et al, 2006 among others). These results (loss of antibacterial properties at low leachate concentrations for Ag-S2 modified bentonite and loss of antibacterial for Cu-S2 modified bentonite) confirms the presence of a strong antibacterial cation or molecule in interlayer of natural S2 beidellite. It also suggests an interaction between the unknown

antibacterial compound and copper, involving in copper retention in interlayer because of evidences of Cu^{2+} and Ag^+ presence in smectite interlayers (decrease of bioavailability). S2 smectitic phase has probably better affinity for the unknown antibacterial agent than for Cu^{2+} and Ag^+, explaining why antibacterial activity is observed only for strong concentration in silver doped S2 and never for copper.

In any case, mechanisms of antibacterial activity for Cu^{2+} and Ag^+ are well known and increased MIC and MBC as observed for Rema sample was expected (Zhao et al, 2006, Malachova et al, 2009, Magaña et al, 2008, Malachova et al, 2011, Hu et al, 2006 among others). Furthermore, Rema bentonite also contains clinoptilolite, which has high CEC. The antibacterial activity observed with these two antibacterial agents comes from this phase too (Top et al, 2003). Their effect is due to bio-availability through exchange of these cations from the interlayer to the leachate. Their interactions with cell wall induce generation of reactive oxygen species (ROS) like hydroxide radicals. These ROS create an oxidative stress to the bacteria and damage cell component like membranes, peptidoglycan layer (for gram + bacterias), proteins, genetic materials etc… (Jiang et al 2016) In addition, physical interactions between nano-clay particles still containing silver or copper in their interlayers probably also create a clustering-effect, giving more efficiency to these antibacterial agents because of proximity. The specific case of S2 bentonite suggests strong interactions in the interlayer between an unknown antibacterial component and copper, reducing their bioavailability and decreasing their antibacterial properties.

ii)   Effect of Aluminium and Boron on antibacterial properties

During doping process, Aluminium and Boron can interact with clay edges and surfaces and are present in porous water. It means that if natural clay has antibacterial properties coming from a compound contained in the interlayer, it will not be exchanged. But this compound can also be released in water during doping process and exchanged with water. In any case, if Boron and/or Aluminium have antibacterial properties, they will be added to Rema or S2 bentonites natural properties.

Concerning Rema Montmorillonite, both Aluminium and Boron induce stronger bacteriostatic and bactericidal properties (figure 17). Except for *K. pneumoniae*, Aluminium efficiency is higher at high and middle leachate concentrations, suggesting that an important quantity of bioavailable aluminium is needed to offer strong and efficient antibacterial effect. Concerning *K. pneumoniae*, aluminium efficiency is only important at high leachate concentration, suggesting this specie is able to react in case of moderate antibacterial attack. Its low resistance in case of low leachate concentration also suggests this bacteria needs to reach a specific concentration of antibacterial agent or needs time to develop its shielding mechanism against the attack. An assumption about this shield can be extracellular polymeric substance synthesis. This assumption will be discussed more in details later. Boron confers bacteriostatic and bactericidal properties at middle concentration (MBC = 50 mg/mL for *S. aureus* and *P. aeruginosa* MBC=100 for *E. coli*) and at high leachate concentration for *K. pneumoniae*, suggesting once again a shielding mechanism for this specie. It confirms results from Photos-Jones et al. 2015. Because of buffering effect of bentonites, the pH of leachate is below 9, suggesting that Boron is present in boric acid form. Boric acid antibacterial effects has been reported by Yimalz 2012 and the observed higher resistance of gram - *E. coli* and *K. pneumoniae* confirms his results on gram dependent antibacterial effect. According to Yimalz, 2012 and Photos-Jones et al, 2015, boric acid mechanism of action is probably based on boric acid diffusion into cell membranes before damaging internal cell components. Unexpectedly, our results with B-modified Rema bentonite does not confirm their results concerning lower resistance for gram + bacteria. But according to Yimalz 2012 results concerning bactericidal effect of boric acid, MBC should be nearly twice higher for *P. aeruginosa* than for *S. aureus.* If our results are similar for *S. aureus* (MBC=66.7 mg/mL), it is not the case for *P. aeruginosa* having same MBC than *S. aureus.* In addition, because MBC = 100mg/mL for *E. coli* and MBC=200 mg/mL for *K. pneumoniae* and because *K. pneumoniae* is also able to resist to other antibacterial agents, it follows

that these two species are able to develop shielding protection against boric acid attack. Because these results are in contradiction with Yimalz 2012, it is possible that our *P. aeruginosa* shows an unexpected sensibility to Boric acid or that Yilmaz 2012's *P. aeruginosa* shows, in contrary, an unexpected shielding ability toward boric acid. Another possible explanation is that boric acid has another mechanism of action than membrane diffusion e.g. cell component damaging as suggested in Photo-Jones et al, 2015. Such mechanism implies greater resistance in gram + species because of their thicker cell wall, which is not coherent with Yimalz 2012 results and ours. As a possible mechanism of action, the action of pump-proteins in membranes can be suggested explaining boric acid entrance in the cell. Furthermore, boric acid bears labile protons that are able to create acidic stress for bacteriae causing membranes damages and finally death. This assumption is supported by the fact that membranes of both gram+ and gram- bacteriae contain weakly acidic functions that are able to attract protons. These protons induce a displacement of structural calcium and magnesium cations in the membrane, inducing instability and better affinity for clay nanoparticles. It is also coherent with a shielding process through Extracellular Polymeric Substances which are able to immobilize toxic particles for *E. coli* and *K. pneumoniae.*

More specifically for S2 bentonite, the aluminium doesn't have significant antibacterial properties for concentrations inferior to 66.7 mg/mL for *S. aureus, E. coli, K. pneumoniae* and does not show any antibacterial property for *P. aeruginosa* (figure 17). Compared to natural S2 bentonites antibacterial capacities, it suggests once again a natural antibacterial compounds in interlayer that is released in water during the doping procedure. Antibacterial properties are observed for aluminium modified Rema against these bacteriae. Consequently, it also suggests that aluminium bioavailability is reduced because of an interaction with the "unknown natural antibacterial component" present in S2 beidellite interlayers.

Boron shows once again good bactericidal and bacteriostatic properties toward tested bacteriae. For *E. coli,* its efficiency is higher at low leachate concentration, and the inverse behaviour is observed for the other species. Furthermore, boron has no antibacterial effect at low concentrations toward *S. aureus* and *P. aeruginosa,* and very low effect against *K. pneumoniae* but it has strong bacteriostatic, and nearly bactericidal effect at very low leachate concentration against *E. coli*. Once again, MBC and behaviour of *P. aeruginosa* and *S. aureus* are similar, suggesting that the B- modified Rema bentonite results are coherent and confirming that another mechanism of action than simple diffusion through cell membrane is involved in boric acid antibacterial activity. The higher resistance of *E. coli* and *K. pneumoniae* suggests once again a shielding mechanism.
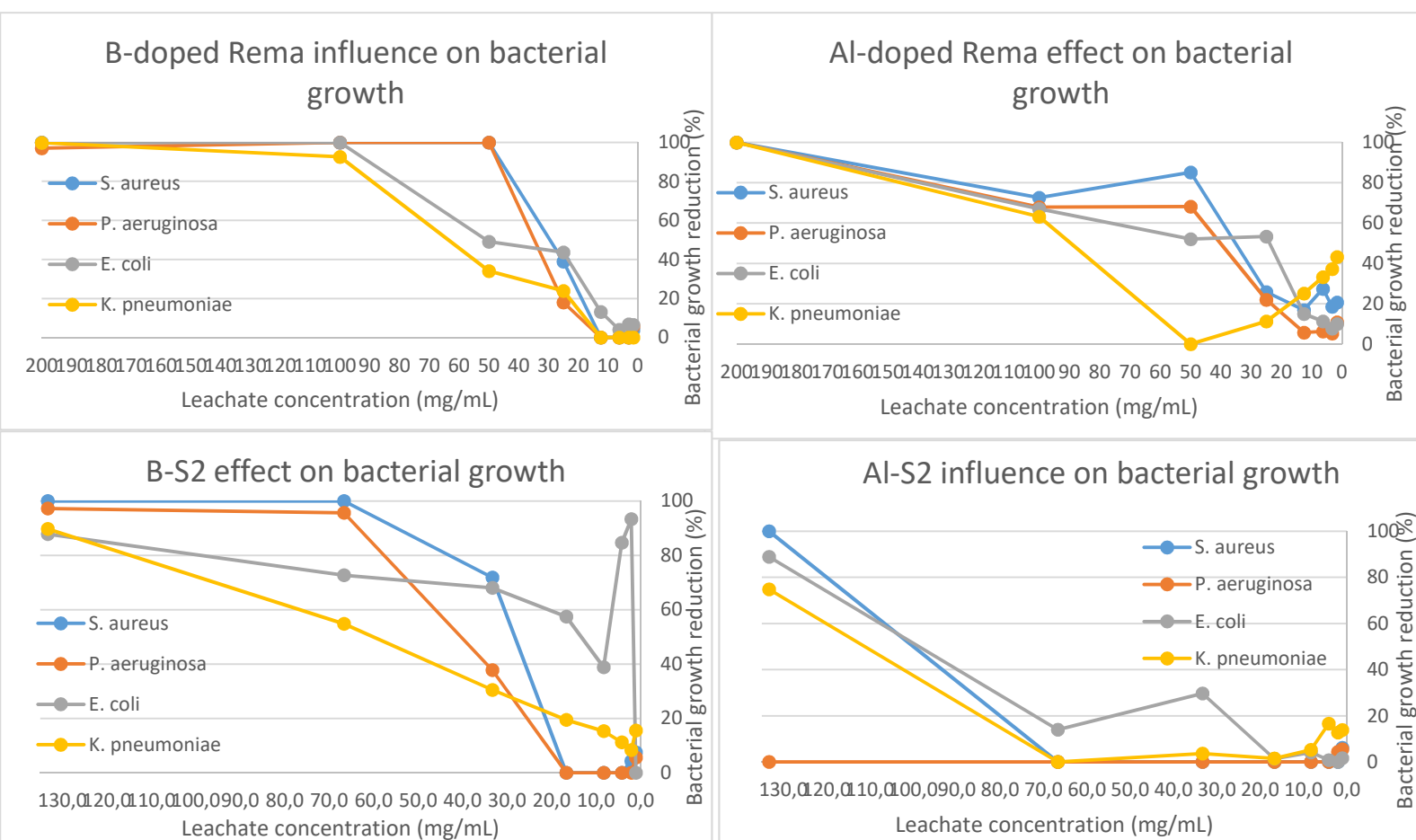
Figure 17: Antibacterial effect of boron and aluminium modified Rema Bentonite and S2 bentonite

iii) Impact of aluminium, boron, silver and copper on MIC and MBC

MIC50 corresponds to Minimum Inhibitory Concentration with bacterial growth reduction of 50%. This value has been traditionally used because it is the observable MIC observable by the naked eyes. However, in some cases, bacteriostatic and bactericidal properties are very strong and MIC50 cannot be defined because bacterial growth reduction is always superior to 50%. Consequently, MIC90, corresponding to bacterial growth reduction of 90% has also been defined. This MIC corresponds to very strong bacteriostatic effects.
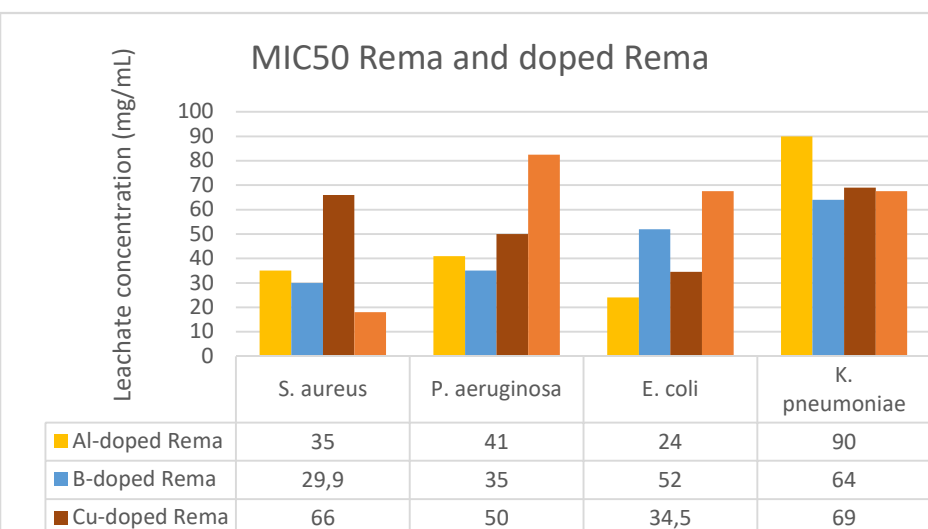

	S. aureus	P. aeruginosa	E. coli	K. pneumoniae
Al-doped Rema	35	41	24	90
B-doped Rema	29,9	35	52	64
Cu-doped Rema	66	50	34,5	69

Figure 18: MIC 50 of Rema bentonite and Rema modified Bentonites

The Ag-Rema bentonite doesn't appear on MIC50 histogram because its bacteriostatic effect is so strong that it induces a bacterial growth reduction superior to 50% regardless of the leachate concentration. It is the strongest bacteriostatic tested agent, at low middle and high leachate concentrations. As supposed in the previous part, *K. pneumoniae* probably develops shielding mechanism against all tested antibacterial agents and also

against natural Rema bentonite antibacterial abilities, explaining similar MIC50 for B-Rema, Cu-Rema and Rema. This shielding mechanism seems to be more efficient against Aluminium.

After Ag-Rema bentonite, the most efficient material against gram + bacteria *S. aureus* is natural Rema suggesting that the higher the physical interactions between gram + cell wall and clays and the higher the uptake of vital elements from culture media, the higher the bactericidal properties towards gram + bacteriae. *P. aeruginosa* and *E. coli* are better deactivated by all doped materials. Efficiency ranking is the following for *P. aeruginosa*: Ag-Rema > B-Rema > Al-Rema > Cu-Rema > Rema and the following for *E. coli*: Ag-Rema > Al-Rema > Cu-Rema > B-Rema. All of them except Ag have bacteriostatic effect. Actually, Ag can be seen as only bactericidal.

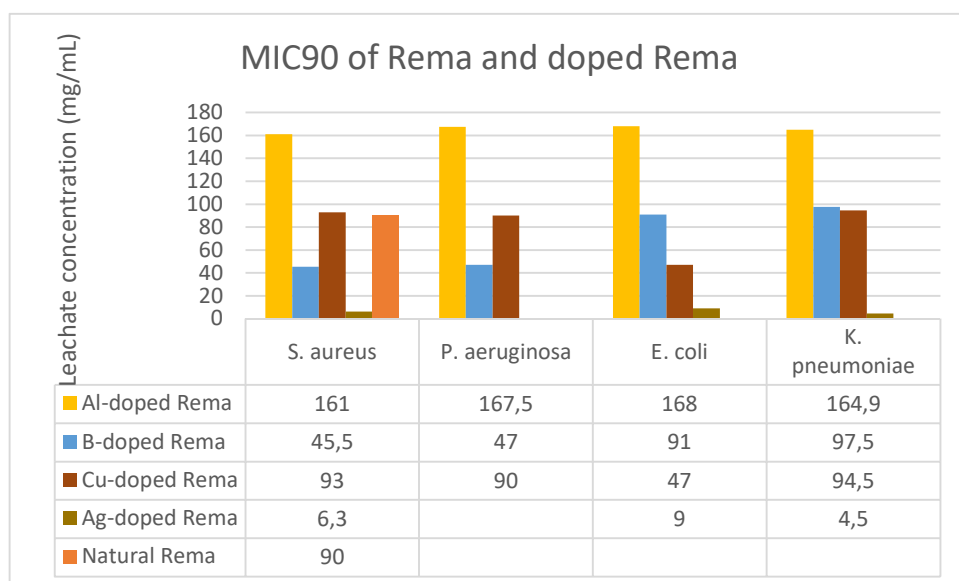By comparison to MIC50, MIC90 shows totally different rankings:

MIC90 of Rema and doped Rema	S. aureus	P. aeruginosa	E. coli	K. pneumoniae
Al-doped Rema	161	167,5	168	164,9
B-doped Rema	45,5	47	91	97,5
Cu-doped Rema	93	90	47	94,5
Ag-doped Rema	6,3		9	4,5
Natural Rema	90			

Figure 19: MIC 90 histogram of Rema bentonite and modified Rema bentonites

If Ag-Rema is still the most efficient material, Natural Rema bentonite is not able to reduce bacterial growth of 90% except for *S. aureus* which confirms the gram-dependant effect of this montmorillonite. In addition, Al-Rema is the less efficient bacteriostatic agent against all bacteriae (MIC90 are higher than 160mg/mL). Boron still has a great efficiency, especially towards *S. aureus* and *P. aeruginosa* (MIC90=45.5 mg/mL and MBC90=47 mg/mL respectively) and it is the second most efficient for these species.

Its efficiency is two times lower for *E. coli* and *K. pneumoniae* and this difference is probably due to the shielding mechanism mentioned before. For these two species, Cu-Rema is the second most efficient, before Boron. So, depending on bacteriostatic effect needed (strong, or moderate), and depending on the application (with high or low concentration of antibacterial agent), and on targeted species (gram type and potential natural resistance), the antibacterial agent has to be carefully selected.
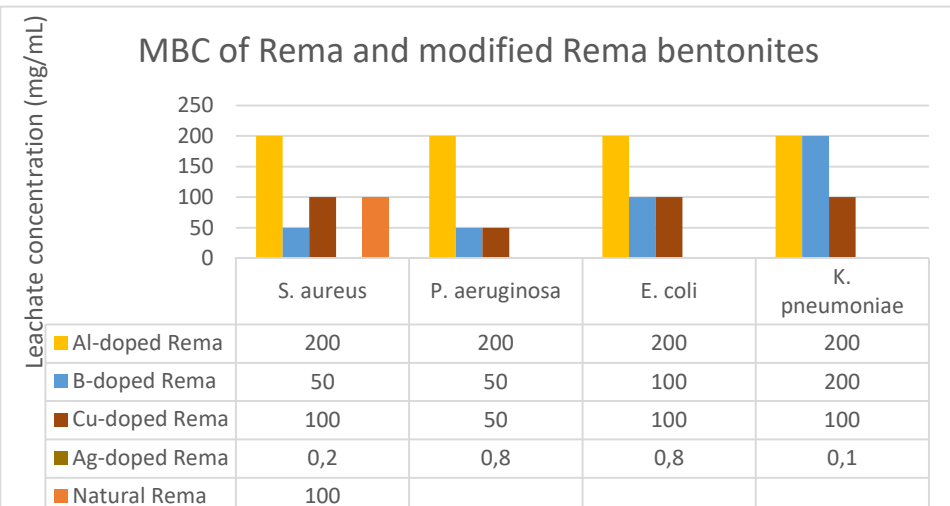
MBC of Rema and modified Rema bentonites

Leachate concentration (mg/mL)

	S. aureus	P. aeruginosa	E. coli	K. pneumoniae
Al-doped Rema	200	200	200	200
B-doped Rema	50	50	100	200
Cu-doped Rema	100	50	100	100
Ag-doped Rema	0,2	0,8	0,8	0,1
Natural Rema	100			

Figure 21: Minimum Bactericidal Concentration of Rema bentonite and modified Rema bentonites

MIC50 of S2 and modified S2 bentonites

Leachate concentration (mg/mL)

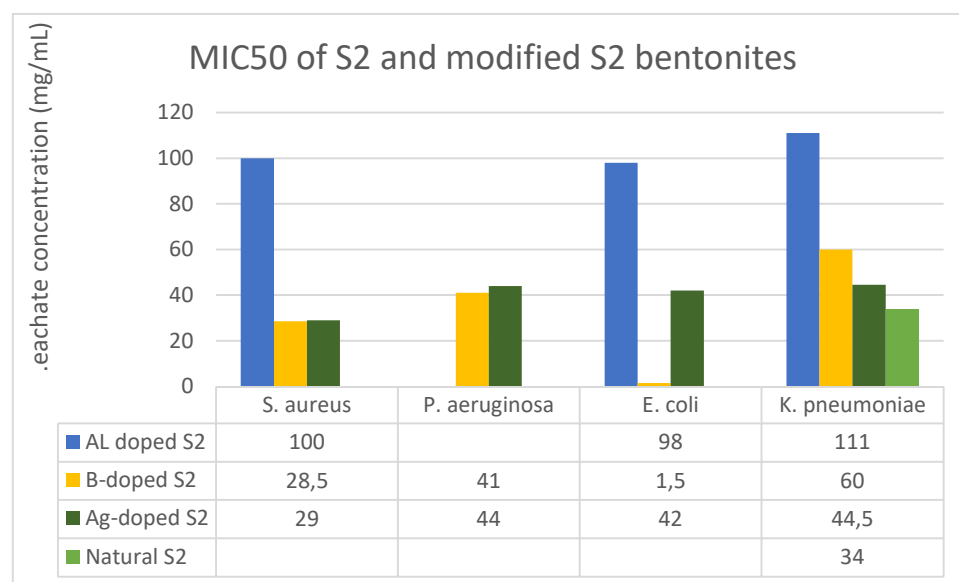|	S. aureus	P. aeruginosa	E. coli	K. pneumoniae
AL doped S2	100		98	111
B-doped S2	28,5	41	1,5	60
Ag-doped S2	29	44	42	44,5
Natural S2				34

Figure 20: Minimum Inhibitory Concentration (50% bacterial growth reduction) of S2 bentonite and modified S2 bentonites

MIC90 of S2 and doped S2 bentonites

Leachate concentration (mg/mL)

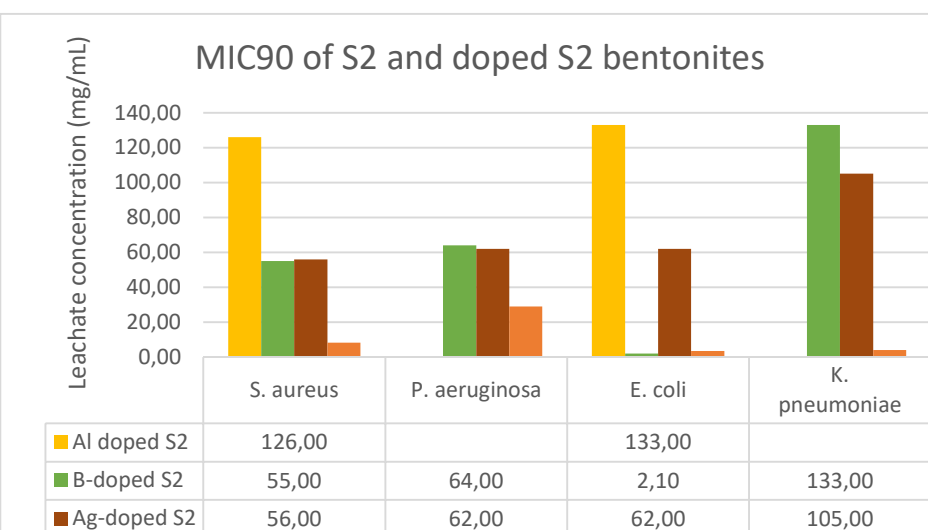|	S. aureus	P. aeruginosa	E. coli	K. pneumoniae
Al doped S2	126,00		133,00	
B-doped S2	55,00	64,00	2,10	133,00
Ag-doped S2	56,00	62,00	62,00	105,00

Figure 22: MIC90 of S2 bentonite and modified S2 bentonites

Concerning bactericidal effect, the most efficient material is Ag-Rema again. Natural Rema bentonite has bactericidal properties only against *S. aureus* confirming its gram dependant effect. Al-Rema, Cu-Rema and B-Rema show bactericidal effect and the less efficient is, again, Al-Rema. B-Rema and Cu-Rema have the same efficiency against *P. aeruginosa* and *E. coli* and have the inverse efficiency against *S. aureus* and *K. pneumoniae* (B-Rema is twice as much efficient than Cu-Rema against *S. aureus* and the inverse is observed for the latter). Except for the Ag-Rema bentonite, bactericidal effect is observed from middle (50 mg/mL) to high (100 mg/mL) leachate concentration. This suggests that Ag-Rema has more bactericidal than bacteriostatic effect and the other are able to have bacteriostatic and bactericidal effect depending on used concentration.

In S2 bentonite and doped S2 materials, the presence of a natural antibacterial agent involves totally different results.

Actually, natural S2 bentonite has only bactericidal (or very strong bacteriostatic) properties, except in the case of *K. pneumoniae* which can be related to its probable shielding mechanism.

Cu-S2 is not present in MIC50, MIC 90 and MBC histograms because it is totally inefficient as an antibacterial agent with this specific beidellite. It is highly probable that the "natural unknown antibacterial compound" reduces its bioavailability.
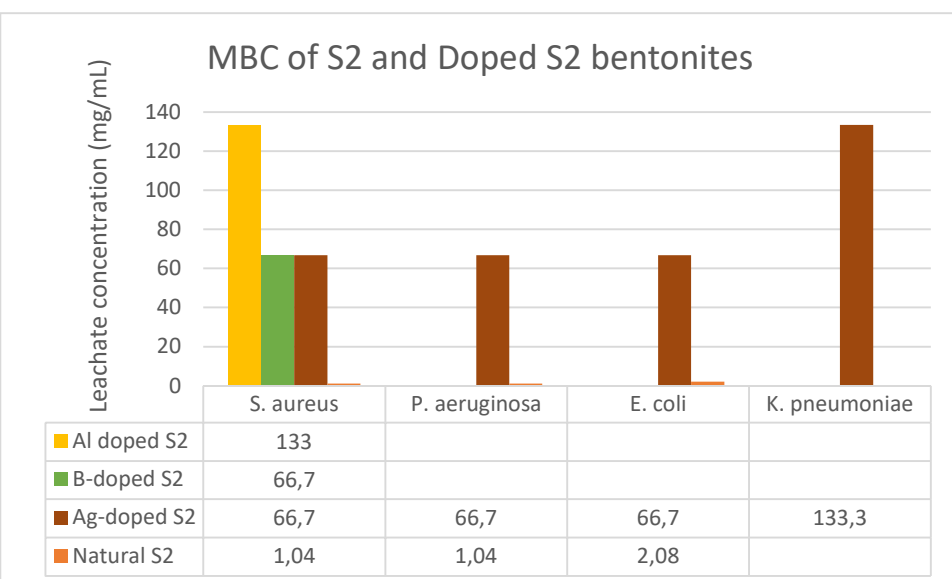
34

MBC of S2 and Doped S2 bentonites

	S. aureus	P. aeruginosa	E. coli	K. pneumoniae
Al doped S2	133			
B-doped S2	66,7			
Ag-doped S2	66,7	66,7	66,7	133,3
Natural S2	1,04	1,04	2,08	

Figure 23: Minimum Bactericidal Concentration of S2 bentonite and modified S2 bentonites

Al-S2 has not enough strong bacteriostatic properties against *P. aeruginosa* to figure on MIC50 histogram and on MIC90 histogram (figure 21 and 22) for *P. aeruginosa, E. coli,* and *K. pneumoniae.* It only shows bactericidal activity against *S. aureus,* suggesting either a gram-type dependence, or lower bioavailability. Because gram dependence was not clearly noticeable with Al-Rema material, the assumption of bioavailability is favoured.

Only Boron and silver have enough bioavailability to offer bacteriostatic properties at middle to low concentration. Ag-S2 seems a slightly more efficient on gram + bacteriae, but, because of the unexpected presence of natural antibacterial agent with unknown effect, conclusion about it is not possible. B-S2 is particularly efficient against *E. coli* and has similar bacteriostatic effect than Ag-S2 against *S. aureus* and *P. aeruginosa.* The inverse behaviour and for twice higher leachate concentration is observed against *K. pneumoniae.* Behaviour between MIC50 and MIC90 are similar unlike Rema based materials, suggesting a more linear relation between concentration and bacteriostatic effect.

The bacteriostatic rankings is Natural S2 > Ag-S2 ~ B-S2 > Al-S2 >> Cu-S2 and the bactericidal ranking is Natural S2 > Ag-S2 > B-S2 >> Al-S2 >> Cu-S2. Because the rankings does not change significantly between the bacteriostatic and bactericidal effect, it suggests that antibacterial properties of S2 and doped-S2 has more linear concentration dependence than for Rema and doped Rema. Possible assumptions are: Influence of charge distribution, or presence of a natural unknown antibacterial compound in S2 bentonite or both of them. Finally concerning S2 and doped S2 materials, the better choice is probably to use it naturally. It will be discussed more in details below.

c)   Kinetics of light effect on silver-doped S2

Because of time and material constrains, light effect on silver doped samples is tested only with Ag-S2. This one has been chose despite its strange behaviour because two mechanisms induced by light are possible. First of all, photo-induced silver reduction to silver nanoparticles might decrease its bioavailability but silver nanoparticles also have great antibacterial effect. A second effect of light is the generation of hydroxyl radicals because of photocatalysis or photo-Fenton reactions. These highly reactive radicals have strong bactericidal and bacteriostatic effect. It is not possible to expect a tendency because of these antagonist mechanisms, coming from the same reaction. Because of these uncertainties, Ag-S2 is selected for
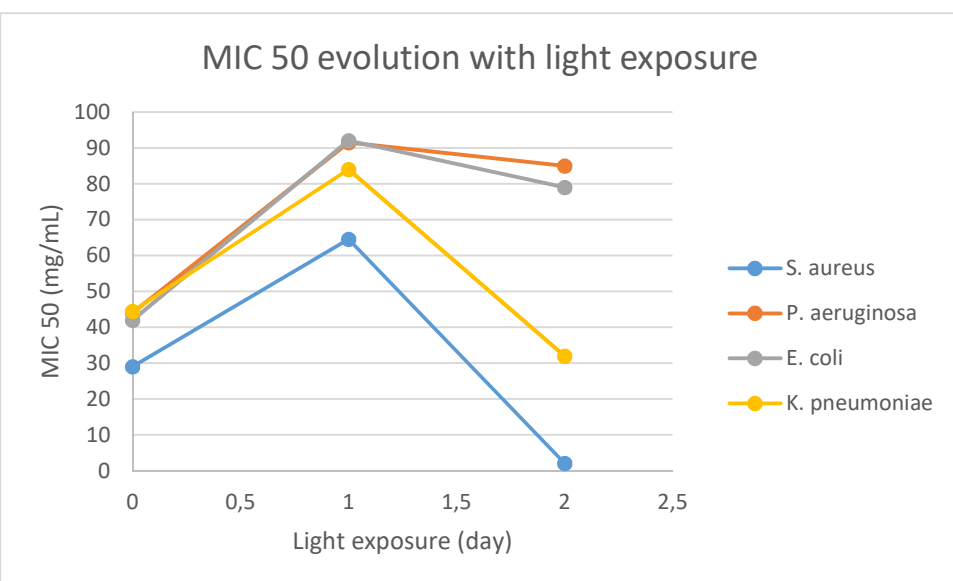

Figure 24: Precipitation of silver nanoparticle after 24h exposition to room-light.

MIC 50 evolution with light exposure

Legend: S. aureus, P. aeruginosa, E. coli, K. pneumoniae

Figure 25: Evolution of the antibacterial properties of Ag-S2 bentonite in function of the light exposition duration

its initial moderate antibacterial effect. Ag-Rema is so strong that an increase in antibacterial properties will not be easy to see.

The first observation is the fast appearance of silver nanoparticles in the leachate (figure 24, 24 hours room-light exposition). The MIC 50 of tested bacteriae demonstrates that Ag-S2 bentonite is sensitive to light exposition (figure 25). Actually, after 24 hours room-light exposition, the MIC50 of all tested bacteriae are doubled, confirming that silver nanoparticles are less bioavailable than silver cations. Another day of light exposition induces an inversion of this tendency: the MIC50 of *P. aeruginosa* and *E. coli* are slightly decreased and the MIC50 of *S. aureus* and *K. pneumoniae* are lower than the MIC50 without light exposition. This suggests that ROS generation is probably high enough to have a significant antibacterial effect combined to silver nanoparticles. A last MIC50 (6 days under room-light) is currently realised and results will be shown during the presentation. The first answer that is possible to give concerning the light action on Ag-S2 bentonite is a two steps tendency. During the first hours of light exposition, light induces silver cations reduction into silver nanoparticle that have less bioavailability. The decrease of bioavailability induces the diminution of Ag-S2 bentonite antibacterial effect towards all tested bacteriae. There are still antibacterial properties that can be explained by the antibacterial properties of silver nanoparticles. These results also suggest that silver cations have greater antibacterial properties than silver nanoparticles. In a second step, light exposition induces the generation of reactive oxygen species through photocatalysis and photo-Fenton reactions, which explains the increase of Ag-S2 efficiency. This effect is particularly efficient toward *K. pneumoniae* and *S. aureus*. Once again, *P. aeruginosa* and *E. coli* are probably able to develop a shielding mechanism that is able to immobilise the ROS.

General interpretation and Discussion

Both supplied samples for the development of an antibacterial litter are bentonites. Rema is a poor quality K-bentonite coming from volcanic ash alteration with water in Milos Rema deposit. It contains about 30% of dioctahedral Smectite but its CEC is quiet big because of Clinoptilolite presence. These two phases confer good adsorption properties. Smectite phase is characterised as low charge Montmorillonite belonging to group 1a and contains about 60% of Montmorillonite-type layers and 40% of Beidellite-type layers. Its low charge and charge distribution does not allow Rema bentonite to form stable suspension in water. Finally, this sample shows low to moderate natural antibacterial properties.

Rema bentonite doped with exchangeable or non-exchangeable cations has enhanced antibacterial properties. The best one is Silver exchanged Rema bentonite but all of them have interesting bacteriostatic and/or bactericidal properties that are concentration-dependent. This latter characteristic is very interesting because, depending of desired efficiency, a dopant can be easily selected. For example, Ag-Rema is dedicated to bactericidal objectives, and Al-Rema will be more

interesting in the case of dilute environment, or for moderate antibacterial efficiency, or as bacteriostatic agent in a concentrated environment. B-Rema and Cu-Rema are also really interesting as bactericidal agents like Ag-Rema but will be more dedicated to concentrated environments with low water activity.

In the leachate obtained from Rema bentonite and modified Rema bentonites, exchangeable cations and nanoclay particles are present. Its natural moderate antibacterial properties are probably linked to the uptake of vital elements in bacteria's environment and to physical interactions between clay nanoparticles and bacterial cell-wall.

S2 bentonite is a higher quality bentonite containing more than 70% of dioctahedral low charge Smectite. Layer charge is mainly located in tetrahedral sheets, meaning its Smectite phase is mainly composed of Beidellite. This sample also shows great colloidal properties that are confirmed by the calculated mean structural formula, which informs it is a Na-Bentonite. In addition, this sample has strong natural antibacterial properties that are associated to a component situated in beidellite interlayer. The interlayer position of this unknown component is strongly supported by the inefficiency of S2 materials doped with exchangeable cations. It also suggests that this component interacts with cations and decreases their bioavailability. The organic or inorganic nature of this compound is unknown for the moment but could be assessed by testing natural S2 after organic removal (chemical oxidation with Sodium Hypochlorite is suggested because it is less toxic against bacterial communities) and MIC/MBC measurements exactly like in this study.

K. pneumoniae and *E. coli* are often able to resist to higher antibacterial agent concentrations suggesting a dose- or time-dependent shielding mechanism, probably based on extracellular polymeric substance synthesis (EPS). The presence of EPS may be verified with electronic microscopy and photography of bacteriae' surfaces.

In addition, higher precision concerning smectite structural formula of both bentonites is possible with EDX analyses under Scanning Electron Microscope. Furthermore, Rema smectitic phase charge distribution is an average of very low intensities peak on broad patterns. It comes from its Montmorillonite content, but does not allow the calculation of precise charge distribution. More than ten Li-saturated XRD patterns have been recorded and only three was reliable. It confirms that Li-saturated Montmorillonite are very complicated to disperse and that an alternative will be welcome for more reliable layer charge distribution estimation.

As it has been explored by Christidis et al, Cesium saturation is dependent on layer charge and on charge distribution, meaning it is not a viable alternative to study a smectite phase with unknown layer charge. In addition, it does not allow studying layer charge distribution between smectite phases having different layer charges. But, knowing layer charge, it is possible to obtain indication concerning charge distribution with such saturation and it would be even more precise for two smectites having same (or nearly same) layer charge. Finally, Cesium saturation is a possible alternative to Li-saturation under certain conditions.

Furthermore, silver and copper doped materials have been prepared following cation exchange procedures. It is a long process (one week of contact between clay and silver/copper solution) which is not reliable in industry. Spray procedure corresponds more to an industrial application, but, because of technical inabilities (not enough microplates for antimicrobial investigation) and time constrains, it could not be tested during this internship. Cation exchange procedure gives the most optimistic results. But because of low contact time between sprayed solution and the clay, it is expected that copper and silver doped samples would be less efficient against tested bacteriae that it is reported here.

Conclusion

To conclude this mineralogical and microbiological study, the development of an antibacterial litter, which includes reduction of ammonia emanations, based on the two furnished bentonites is possible. This study clearly demonstrates that the best antibacterial agent is Ag-Rema, but it is a long procedure, with an expensive cation and, silver cytotoxicity is strong. In fact, its mechanism of action through generation of Reactive Oxygen Species is not specific to bacteriae and does not make difference between mammalian cells and bacterial cells. Antibacterial agents prepared with silver, even if they are strongly efficients, are not advised for this specific application because of repeated and direct contact with cat paws and because of swallowing risks. Depending on the company wishes (strong bacteriostatic effect, strong bactericidal effect…) different solutions are possible. Adsorption properties of Rema and S2 bentonites and the low quantity of water from cat urine compared to litter quantity induces a concentrated environment. The best antibacterial agents in this specific application are the most efficient at high leachate concentrations in antibacterial agent. It means that all cation-doped Rema bentonites, and natural S2, and B-S2 are reliable for this application.

 For the specific case of natural S2 bentonite, more tests are needed, especially to identify the natural unknown antibacterial compound present in interlayer. Its toxicity also should be investigated because if it is a viable compound, it is possible to offer a naturally and affordable antibacterial litter which would be easily prepared. Furthermore, it is also probably possible to develop two types of antibacterial cat litter: A clumping litter, based on natural S2 (if it is a non-toxic natural antibacterial agent) because of its strong colloidal properties, giving high sticky characteristics in presence of water and a non-clumping one based on Al-Rema or Cu-Rema modified bentonites.

Boron and derived compounds cytotoxicity are proved (Photo-Jones et al, 2015) but its low ability to penetrate mammalian tissues may allow its use with restrictions in Boron concentration for example or in specific breeding where children are not expected or animals are not known for eating their litter (for example, it could not be a rodent litter). A specific study about this point could be very interesting. Furthermore, because its mechanism of action against bacterial cells seems not totally understood, such study will give the opportunity to clearly define this mechanism.

Finally, because Aluminium is toxic towards mammalian cells (especially intestinal epithelium cells) only with high concentrations (Djouina et al., 2016), it may be a compromised between antibacterial properties and toxicity. Indeed, Al-Rema bentonite would offer correct bacteriostatic effect towards gram + and gram - bacteriae with a minimum of security. Naturally, the best solution would be an evidence of natural S2 non-toxicity.

Acknowledgements

Bibliography

Kohtz et al, 2006
John C. Kohtz, Paul M. Treichel Jr, « Chp. 1 : Le comportement des solutions », <u>Chimie des solutions</u>, p.16-18, Edition Broché, 2006.

Christidis et al, 2003
G. E. Christidis and D. D. Eberl, "Determination of layer charge characteristics of smectites", <u>Clays and Clay Minerals</u>, Vol. 51, No. 6, p.644–655, 2003

Christidis et al, 2006
G. E. Christidis, A. E. Blum, D.D. Eberl, "Influence of layer charge and charge distribution of smectites on the flow behaviour and swelling of bentonites", <u>Applied Clay Science</u>, 34, p. 125-138, 2006

Jaynes & Bigham, 1987
W. F. Jaynes, J. M. Bigham, "Charge Reduction, octahedral charge and lithium retention in heated, Li-saturated smectites", <u>Clays and clay minerals,</u> Vol. 35, N°6, p. 440-448, 1987

Howard, 1981
J. J. Howard, "Lithium and Potassium saturation of Illite/smectite clays from interlaminated shales and sandstones", <u>Clays and clay minerals</u>, Vol. 29, N°2, p. 136-142, 1981

Czímerová et al, 2006
A. Czímerová, J. Bujdák, R. Dohrmann, "Traditional and novel methods for estimating the layer charge of smectites", <u>Applied Clay Science</u>, 34, p. 2-13, 2006

Christidis, 2008
G. E. Christidis, "Validity of the structural formula method for layer charge determination of smectite: a re-evaluation of published data", <u>Applied Clay Science</u>, 42, p. 1-7, 2008

Chowdhurry et al, 2016
N. R. Chowdhury, M. MacGregor-Ramiasa, P. Zilm, P. Majewski, K. Vasilev, "'Chocolate' silver nanoparticles: Synthesis, antibacterial activity and cytotoxicity", <u>Journal of colloid and interface science,</u> Vol. 482, p. 151-158, 2016

Djouina et al, 2016
M. Djouina, N. Esquerre, P. Desreumaux, C. Vignal, M. Body-Malapel, "Toxicological consequences of experimental exposure to aluminum in human intestinal epithelial cells", <u>Food and chemical toxicology</u>, 91, p. 108-116, 2016

Radziun et al, 2011
E. Radziun, J. Dudkiewicz Wilczynska, I. Ksiazek, K. Nowak, E.L. Anuszewska, A. Kunicki, A. Olszyna, T. Zabkowski, "Assessment of the cytotoxicity of aluminium oxide nanoparticles on selected mammalian cells", <u>Toxicology in Vitro</u>, 25, p. 1694-1700, 2011

Van Der Marel et al., 1976
Van Der Marel and H.W. Beutelspracher, <u>Atlas of Infrared Spectroscopy of clay minerals and their admixtures</u>, 1976

Madejova et al, 2011
Madejova et al, <u>EMU notes in mineralogy</u> Vol. 9, chapter 6, p. 171-226, 2011

Villa et al, 2016
T.G. Villa et al, Chapter 2: Resistant and Emergent Pathogenes in Food Products, p. 11-34, <u>Antimicrobial Food Packaging,</u> 2016

Bouchet et al, 2000
A. Bouchet, A. Meunier, P. Sardini, Minéraux argileux : structure cristalline, identification par diffraction de rayons X. – Bull. Centre Rech. Elf Explor. Prod., Mém. 23, 136p., 126 fig., 30tab., Pau 2000.

Jaynes et al, 1987
W. F. Jaynes, J.M. Bigham, "Charge reduction, octahedral charge, and lithium retention in heated, Li-saturated smectites", <u>Clays and Clay Minerals</u>, Vol. 35, N°6, p. 440-448, 1987

J. J. Howard, 1981
James. J. Howard, "Lithium and Potassium saturation of Illite/Smectite clays from interlaminated shales and sandstones", <u>Clays and Clay Minerals</u>, Vol. 29, N°2, p. 136-142, 1981.

Elzea et al, 1994
J. M. Elzea, I. E. Odom, W. J. Miles, "Distinguish well-ordered Opal-CT and Opal-C from high temperature cristobalite by X-ray diffraction", <u>Analytica Chemica Acta</u>, 286, p. 107-116, 1994

Elzea et al, 1996
J.M. Elzea, S. B. Rice, "TEM and X-ray diffraction evidence for cristobalite and tridymite stacking sequences in Opal", <u>Clays and clay minerals</u>, Vol. 44, N°4, p. 492-500, 1996

Guthrie et al, 1995
G. D. Guthrie Jr., D. L. Bish, R. C. Reynolds Jr., "Modelling the X-ray diffraction pattern of Opal-CT", <u>American mineralogist</u>, Vol. 80, p. 869-872, 1995

Miles 1994
W. J. Miles, "Chemical methods of analysis for crystalline silica, a critical literature review", <u>Analytica Chemica Acta</u>, 286, p. 3-7, 1994

Onal et al, 2007
M. Onal, S. Kahraman, Y. Sarikaya, "Differentiation of α-cristobalite from opals in bentonites from Turkey", <u>Applied Clay Sciences</u> 35, p. 25-30, 2007

Hillier et al, 2008
S. Hillier and D. G. Lumdson, "Distinguishing opaline silica from cristobalite in bentonites: a practical procedure and perspective based on NaOH dissolution", <u>Clay Minerals</u>, p. 477-486, 2008

Zilaout et al, 2017
H. Zilaout, J. Vlaanderen, R. Houba, H. Kromhout, "15 years of monitoring occupational exposure to respirable dust and quartz within the European industrial minerals sector", International Journal of Hygiene and Environmental Health, 2017

Dodds, 2017
D. R. Dodds, "Antibiotic resistance: A current epilogue", <u>Biochemical pharmacology</u>, 134, p. 139-146, 2017

Schiffman et al., 1996
P. Schiffman, R. J. Southard, "Cation Exchange Capacity of layered silicates and palagonitized rocks glass in mafic volcanic rock: a comparative study of bulk extraction and *in situ* technics", <u>Clays and clay minerals</u>, Vol. 44, N°5, p. 624-634, 1996

Pepper et al, 2014
Ian L. Pepper, Charles P. Gerba and Terry J. Gentry, <u>Environmental Microbiology</u>, 3rd Edition, 2014

Mathijs, 2015
E. Mathijs, "Exploring future patterns of meat consumption", <u>Meat Science</u>, 109, p. 112-116, 2015

Kaufhold et al, 2017
S. Kaufhold, R. Dohrmann, M. Klinkenberg, S. Siegesmund, K. Ufer, "N2-BET specific surface area of bentonites", <u>Journal of Colloid and Interface Science,</u> 349, p. 275-282

Cui, 2017
Y. J. Cui, "On the hydro-mechanical behaviour of MX80 bentonite-based materials", review paper, <u>Journal of Rock Mechanics and Geotechnical Engineering,</u> 9, p. 565-574

Trevisi et al, 2014
E. Trevisi, A. Zecconi, S. Cogrossi, E. Razzuoli, P. Grossi, M. Amadori, "Strategies for reduced antibiotic usage in dairy cattle farms", <u>Research in Veterinary Science</u>, 96, p. 229-233, 2014

Barast et al, 2016
G. Barast, A.-R. Razakamanantsoa, I. Djeran-Maigre, T. Nicholson, D. Williams, "Swelling properties of natural and modified bentonites by rheological description", <u>Applied Clay Science</u>, 2017

Thiry et al, 2013
M. Thiry, N. Carillo, C. Franke, N. Martineau, « Technique de preparation des minéraux argileux en vue de l'analyse par diffraction aux rayons X et introduction à l'interprétation des diagrammes », 2013

Sans et al, 2015
P. Sans, P. Combris, "World meat consumtion patterns: An overview of the last fifty years (1961-2011)", <u>Meat Science</u>, 109, p. 106-111

Akbar et al, 2017
W. Akbar, M. R. Noor, K. Kowal, T. Syed, T. Soulimane, G. Bahar Basim, "Characterization and antibacterial properties of nanoboron powders and nanoboron powder coated textiles", <u>Advanced Powder Technology</u>, 28, p. 596-610, 2017

Hu et al, 2006
C.-H. Hu, M.-S. Xia, "Adsorption and antibacterial effect of copper-exchanged montmorillonite on Escherichia "coli K88", <u>Applied Clay Science</u>, 31, p. 180-184, 2006

Magaña et al, 2008
S.M. Magaña, P. Quintana, D.H. Aguilar, J.A. Toledo, C. Angeles-Chavez, M.A. Cortés, L. Leon, Y. Freile-Pelegrın, T. Lopez, R.M. Torres Sanchez, "Antibacterial activity of montmorillonite modified with silver", <u>Journal of Molecular Catalysis A: Chemical 281,</u> p. 192-199, 2008

Zhao et al, 2006
D. Zhao, J. Zhou, N. Liu, "Preparation and characterization of Mingguang palygorskite supported with silver and copper for antibacterial behaviour", Applied Clay Science, 33, p. 161-170, 2006

Omara 2017,
S. T. Omara, "MIC and MBC of Honey and Gold Nanoparticles against methicillin-resistant (MRSA) and vancomycin-resistant (VRSA) coagulase-positive *S. aureus* isolated from contagious bovine clinical mastitis", Journal of Genetic Engineering and Biotechnology, Article in press, 2017

Malachova et al, 2011
K. Malachová, P. Praus, Z. Rybková, O. Kozák, "Antibacterial and antifungal activities of silver, copper and zinc montmorillonites", Applied Clay Science, 53, p. 642-645, 2011

Malachova et al, 2008
K. Malachová, P. Praus, Z. Pavlíčková, M. Turicová, "Activity of antibacterial compounds immobilised on montmorillonite", Applied Clay Science, 43, p. 364-368, 2008

Cunha, 2005
B. A. Cunha, "Methicillin-resistant Staphylococcus aureus: clinical manifestations and antimicrobial therapy", Clin Microbiol Infect, 11, (Suppl. 4), p. 33–42, 2005

Photo-Jones et al, 2015
E. Photos-Jones, C. Keane, A.X. Jones, M. Stamatakis, P. Robertson, A.J. Hall, A. Leanord, "Testing Dioscorides' medicinal clays for their antibacterial properties: the case of Samian Earth", Journal of Archeological Science, 57, p. 257-267, 2015

Wang et al, 2014
Y. Wang, X. Xue, H. Yang, "Preparation and characterization of carbon or/and boron-doped titania nano-materials with antibacterial activity", Ceramics International, 40, p. 12533-12537, 2014

Frost et al, 2000
R. L. Frost, H. Ruan, J. T. Kloprogge, W.P. Gates, "Dehydration and dehydroxylation of nontronites and ferruginous smectite", Thermochimica Acta, 346, p. 63-72, 2000

Ding & Frost, 2002
Z. Ding, R.L. Frost, "Controlled rate thermal analyses of Nontronites", Thermochimica Acta, 389, p. 185-193

Onodera et al, 1998
Y. Onodera, T. Iwasaki, T. Ebina, H. Hayashi, K. Torii, A. Chatterjee, H. Mimura, "Effect of layer charge on fixation of cesium ions in smectites", Journal of Contaminant Hydrology, 35, p. 131-140, 1998